Journal of Environmental Chemical Engineering 12 (2024) 114603

Contents lists available at ScienceDirect

Journal of Environmental Chemical Engineering

journal homepage: www.elsevier.com/locate/jece

Support induced effects on the activity and stability of Ga_2O_3 based catalysts for the CO_2-assisted oxidative dehydrogenation of propane

Alexandra Florou [a], Georgios Bampos [b], Panagiota D. Natsi [b], Aliki Kokka [a], Paraskevi Panagiotopoulou [a,*]

[a] Laboratory of Environmental Catalysis, School of Chemical and Environmental Engineering, Technical University of Crete, Chania GR-73100, Greece
[b] Department of Chemical Engineering, University of Patras, Patras GR-26504, Greece

ARTICLE INFO

Keywords:
CO2-assisted oxidative dehydrogenation of propane
Propylene production
Surface basicity/acidity
Ga2O3-TiO2
Ga2O3-SiO2
Ga2O3-Al2O3

ABSTRACT

The influence of the support nature (Al_2O_3, TiO_2, SiO_2) on the activity and stability of supported Ga_2O_3 (10 wt%) catalysts was investigated for the production of propylene through the CO_2-assisted oxidative dehydrogenation of propane (CO_2-ODP). Catalytic activity was found to be higher when gallium oxide was dispersed on alumina support which was characterized by the highest acid site density and moderate surface basicity. Below 650 °C propylene yield increased in the order Ga_2O_3-TiO_2<Ga_2O_3-SiO_2<Ga_2O_3-Al_2O_3, which was modified as Ga_2O_3-Al_2O_3<Ga_2O_3-TiO_2<Ga_2O_3-SiO_2 for higher reaction temperatures. Propylene selectivity decreased with increasing reaction temperature followed by an increase of ethylene and methane selectivity implying that the side reactions of propane hydrogenolysis and propane/propylene decomposition were facilitated at higher temperatures hindering the CO_2-ODP reaction. Gallium oxide catalysts supported on TiO_2 and SiO_2 exhibited sufficient stability for 30-35 hours on stream at 660 and 710 °C, contrary to Ga_2O_3-Al_2O_3 which although was stable at 710 °C it was gradually deactivated when the reaction was taking place at 600 °C. Temperature programmed oxidation experiments showed that carbon deposition was favored over Ga_2O_3-Al_2O_3 catalyst when the reaction was conducted at low temperature, which may be related to the higher surface acidity of this sample and be responsible for its deactivation with time. SEM images and elemental mapping obtained from both the freshly prepared and used Ga_2O_3-M_xO_y samples showed that Ga and M (M: Si, Ti, Al) were uniformly present even after prolonged catalyst interaction with the reaction mixture. EDS analysis indicated that carbon formation was accelerated with increasing reaction temperature.

1. Introduction

The production of propylene (C_3H_6), which ranks among the most critical building blocks for the industrial production of numerous chemical compounds (propylene glycol, propylene oxide, acrolein, polypropylene, acetone etc), can be achieved by employing various processes like Fischer-Tropsch synthesis to olefins, methanol conversion to olefins, steam cracking of naphta, fluid catalytic cracking, thermal dehydrogenation of propane (DP) (1) and oxidative dehydrogenation of propane (C_3H_8) (ODP) (2) [1–3]. The latter two approaches are considered to be attractive due to (a) the abundant availability of propane contained in shale gas condensates which can be easily extracted in large scale and (b) the relatively high propylene selectivity that they can achieve addressing the continuously rising demands for its production [3,4].

$$C_3H_8 \leftrightarrow C_3H_6 + H_2 \qquad \Delta H^0_{298K} = 124.3\ kJ/mol \tag{1}$$

$$C_3H_8 + 1/2O_2 \leftrightarrow C_3H_6 + H_2O \qquad \Delta H^0_{298K} = -117.6\ kJ/mol \tag{2}$$

The ODP process outperforms the thermal DP which suffers from high requirements of thermal energy due to its high endothermicity as well as from thermodynamic restrictions by the operating reaction conditions including feed composition, reaction temperature and pressure [2,5]. However, the use of molecular O_2 as oxidant in the ODP reaction may result in deep oxidation of the produced propylene decreasing its selectivity. Alternatively, the use of a milder oxidant like CO_2 (3) has been proposed as an effective and innovative technology able (a) to address the equilibrium limitations by removing the produced H_2 from the gas stream via the reverse water-gas shift (RWGS) reaction (4) while simultaneously maintaining high propylene selectivity, and (b)

* Corresponding author.
E-mail address: ppanagiotopoulou@tuc.gr (P. Panagiotopoulou).

https://doi.org/10.1016/j.jece.2024.114603
Received 10 June 2024; Received in revised form 19 September 2024; Accepted 28 October 2024
Available online 29 October 2024

to reduce CO_2 emissions, contributing to its utilization and therefore, the mitigation of global warming and climate change [2].

$$CO_2 + C_3H_8 \leftrightarrow C_3H_6 + CO + H_2O \qquad \Delta H^0_{298K} = 165.4\ kJ/mol \qquad (3)$$

$$CO_2 + H_2 \leftrightarrow CO + H_2O \qquad \Delta H^0_{298K} = 41.1\ kJ/mol \qquad (4)$$

Raising of reaction temperature favors the cleavage of both the C-H bond leading to propane dehydrogenation and the C-C bond which enhances side reactions, such as propane cracking towards methane and ethylene or carbon, and propane hydrogenolysis yielding ethane and methane, decreasing propylene selectivity and, in certain cases, promoting carbon deposition [4]. However, CO_2 may also act as decarburization compound removing the so formed coke from the catalyst surface through the reverse Boudouard reaction, thus contributing to the increase of catalyst lifetime. [1,3,6]. It is worth mentioned that depending on the catalyst used the interaction of C_3H_8 with CO_2 may result in syngas (CO/H_2) production via the dry propane reforming reducing propylene yield [1,3]. Therefore, the development of coke-resistance catalysts with tunable properties able to activate both C_3H_8 and CO_2 by promoting the strong scission of C-H bond and the weak cracking of C−C bond leading to high C_3H_6 yields is of great challenge [3,5,6]. Moreover, ODP catalysts should be characterized by high hydrothermal stability in order to inhibit deactivation by the produced H_2O molecules [3].

Several catalyst formulations have been investigated so far for the CO_2-ODP reaction including SiO_2-, Al_2O_3-, TiO_2- and ZrO_2-supported metal oxide catalysts such as Cr_2O_3-SiO_2 [7,8], V_2O_5-SiO_2 [9], Ga_2O_3--SiO_2 [8,10], Cr_2O_3-Al_2O_3 [7,11], VO_x-Al_2O_3 [12] Ga_2O_3-Al_2O_3 [8, 13–16], Cr_2O_3-ZrO_2 [11], Ga_2O_3-TiO_2 [1,8] and Ga_2O_3-ZrO_2 [8,17]. Platinum based catalysts were also found to exhibit high propane dehydrogenation activity due to Pt affinity for paraffinic C-H bonds enabling the superior activation of C-H bond and the weak scission of C-C bond [3,4]. Zeolites were also explored as catalyst supports for the CO_2-ODP reaction and found to be effective materials to disperse metal (e.g. Pt) or metal oxide (e.g. CrO_x, Ga_2O_3) particles due to their high specific surface area, uniform and well-ordered micro- or mesoporous-channels with control pore sizes and excellent hydrothermal stability [3,5,18–20].

Among the investigated catalysts those containing gallium oxide either as the active phase or as a support component were found to exhibit exceptional activity for the oxidative dehydrogenation of propane due to Ga_2O_3 ability to control the physicochemical properties of catalyst, especially surface acidity and basicity, as well as to facilitate the activation of C-H bond by a non-redox pathway [4,21,22]. According to this scheme CO_2 participates in H_2 consumption via the RWGS (4) and contributes to equilibrium position shift leading to higher C_3H_6 yields [14]. It should be noted, however, that some researchers suggested that the Mars-van Krevelen mechanism may also be applicable over gallium containing catalysts according to which the lattice oxygen ions act as the selective oxygen species and the oxygen vacancies as the adsorption sites with CO_2 participating in the re-oxidation of the partially reduced $Ga^{\delta+}$ ($\delta < 2$) [15]. Moreover, some research groups were focused on the development of metal oxide-supported Ga_2O_3 catalysts employing alternative methods such as the atomic layer deposition method which was found to be beneficial compared to the wet impregnation method, at least over Ga_2O_3-Al_2O_3 catalysts, due to the induced increase of Ga_2O_3 dispersion and enhancement of Ga_2O_3-Al_2O_3 interaction leading to the formation of Ga-O-Al linkages and improved surface acidity [14]. The hydrothermal synthesis method was also proposed as an effective method for the preparation of Ga_2O_3-Al_2O_3 catalysts leading to high specific surface area, high number of tetrahedral Ga ions and medium-strong Lewis acid sites and thus, to superior activity for the CO_2-ODP reaction [15].

In our recent study, the CO_2-ODP reaction was investigated over various metal oxides supported on TiO_2 (M_xO_y-TiO_2, M: Zr, Ce, Ca, Cr, Ga). A significant increase of both propane conversion and propylene yield was demonstrated with the Cr_2O_3 and Ga_2O_3 containing catalysts exhibiting superior performance. A synergistic effect between M_xO_y and TiO_2 was found to occur leading to modification of the physicochemical properties of catalysts including the surface acidity and basicity, the reducibility, the anatase/rutile content and the primary crystallite size of TiO_2 support which affect catalytic activity and propylene yield. Among these characteristics a moderate surface basicity and small titania crystallite size were found to be desirable in order to achieve high propane conversion and propylene yield. *In situ* FTIR spectroscopy experiments conducted under reaction conditions indicated that the adsorption/activation of CO_2 was facilitated with the addition of metal oxides on TiO_2 surface due to the improved surface basicity leading to higher C_3H_6 yields.

In the present study, the influence of the support nature (Al_2O_3, TiO_2, SiO_2) on the activity and stability of supported Ga_2O_3 (10 wt%) catalysts was investigated for the CO_2-assisted oxidative dehydrogenation of propane. The correlation of physicochemical properties with catalysts' ability to convert propane towards propylene was explored and discussed in detail. The time on stream (TOS) stability of the synthesized catalysts was investigated at various reaction temperatures, whereas advanced surface characterization of both the freshly prepared and used samples (denoted in the following as "fresh" and "spent") was carried out in order to understand the catalysts' tendency to coke formation and possible deactivation phenomena. The new findings of the present study lie in the following key points: (a) Identification of the support role and the key physicochemical characteristics that determine catalytic activity and stability; (b) the development of active catalysts with sufficient stability for 30–35 hours on stream contrary to previous studies where a rapid catalyst deactivation was observed and (c) the determination of catalyst properties following prolonged interaction of catalyst with the CO_2/C_3H_8 mixture and their correlation with the promotion of undesired reactions.

2. Materials and methods

2.1. Catalysts synthesis and characterization

Gallium based composite metal oxides (10 %Ga_2O_3-M_xO_y) were synthesized employing the incipient wetness impregnation method using commercial SiO_2 (Alfa Aesar), TiO_2 (Evonik) or Al_2O_3 (Alfa Aesar) as supports and $Ga(NO_3)_3{\cdot}6\ H_2O$ (Sigma Aldrigh) as the precursor of gallium oxide. The procedure involved dissolution of the appropriate amount of $Ga(NO_3)_3{\cdot}6\ H_2O$ in water followed by the addition of the suitable support amount. The volume of the precursor solution per mass of support used was in all cases equal to 11. The resulting slurry was progressively heated at 80 °C under continuous stirring and maintained at that temperature until water evaporation. The remained solid was dried at 120 °C overnight and calcined in air at 600 °C for 3 hours.

Brunauer-Emmett-Teller (BET) method following N_2 physisorption at liquid nitrogen temperature conducted on a Gemini III 2375 instrument (Micromeritics) was used to estimate the specific surface area (SSA) of the supported gallium oxide catalysts following the procedure described in the Supplementary Material. The phase identification analysis of the synthesized catalysts was carried out by X-Ray Diffraction (XRD) technique using a Bruker D8 Advance instrument operated at 40 kV and 40 mA with a Cu-Kα radiation (λ= 0.15496 nm) source and a scan rate of 0.05 °/s. Comparison of the diffraction peaks with those supplied by the JCPDS data base enabled their identification. The catalysts' surface basicity was investigated by temperature-programmed desorption of CO_2 (CO_2-TPD) experiments in a fixed bed reactor using an Omnistar (Pfeiffer Vacuum, Asslar, Germany) mass spectrometer (MS) directly connected with the reactor outlet and following the procedure described in detail in our recent study [1]. The same reactor/-instrumentation was utilized for the investigation of catalysts' reducibility by temperature-programmed reduction with H_2 (H_2-TPR) as

well as the possible carbon deposition on the catalyst surface under reaction conditions by means of temperature-programmed oxidation (TPO) experiments [1,23]. The surface basicity was also studied by in situ diffuse reflectance infrared Fourier transform spectroscopy (DRIFTS) performed on a FTIR (Nicolet iS20, Thermo Fischer Scientific) spectrometer (operating with a MCT detector and a KBr beam splitter), which was directly connected with a flow measuring system enabling the desired gas mixture composition to be provided to the diffuse reflectance cell where the catalyst was placed [1].

Thermogravimetric analysis (TGA) experiments were conducted under N_2 atmosphere on a TA Q50, Thermal Analysis instrument (TA instruments/WATERS) to determine the surface acidity of the gallium oxide based catalysts after ammonia adsorption following the procedure described in detail elsewhere [1]. In an attempt to identify the nature of acid sites, pyridine adsorption experiments combined with FTIR spectroscopy were carried out using the FTIR spectrometer described above. The experimental procedure involved overnight drying of catalyst powder at 110 °C prior to its saturation with pyridine for 2 h at 25 °C using a 5 %Pyridine/H_2O solution (Sigma Aldrich). The suspension was then filtered and the solid residue was evacuated at 60 °C for 1 h to remove water and physisorbed or weakly chemisorbed pyridine. The catalyst was then placed in the DRIFT cell and the spectrum was collected at 25 °C by subtracting the background spectrum of the corresponding sample that had been previously dried at 110 °C overnight.

A Transmission Electron Microscope (TEM) (JEOL JEM-2100) operated at 200 kV (point resolution 0.23 nm) using an Erlangshen CCD Camera (Gatan Model 782 ES500W) was used to explore the morphology of both "fresh" and "spent" composite metal oxides. The formed crystallographic structures as recorded in TEM images were furtherly analyzed employing selected area electron diffraction (SAED) technique [23]. Scanning Electron Microscopy (SEM) images were also collected on a JEOL JSM 6300 microscope which was equipped with an energy dispersive spectrometer (EDS) for elemental analysis [24].

2.2. Catalytic performance tests

The CO_2-ODP reaction was performed in a fixed bed cylindrical reactor (length of 45 cm, I.D.: 4 mm) made of quartz in the temperature range of 500–750 °C under ambient pressure. In a typical experiment, the catalyst (0.5 g) was sieved to obtain a uniform particle size of 0.15–0.25 mm and placed in an expanded section of 5 cm length (I.D.: 10 mm) in the middle of the reactor where a small amount of quartz wool was placed to immobilize the catalyst powder. Prior to the reaction onset the catalyst was treated in He at 450 °C for 1 hour. Subsequently, the temperature was increased at 500 °C and a gas stream of 5 % C_3H_8+25 %CO_2/He was introduced into the reactor with a total flow rate of 50 cm^3 min^{-1} regulated by using mass-flow controllers. Reactants and products were analyzed after 30 minutes of catalyst on stream on a gas chromatograph (GC Shimadzu 2014) online connected with the reactor outlet. The gaseous products CO, CO_2 and CH_4 were separated using a packed Carboxen column and detected by a thermal conductivity (TCD) detector, whereas C_3H_8, C_3H_6, C_2H_6 and C_2H_4 were separated by a packed Porapak-Q column and detected by a flame ionization detector (FID). A stepwise increase of temperature up to 750 °C was then followed and a similar analysis was carried out at the desired reaction temperatures. A K-type thermocouple was used to measure the temperature in the middle of the catalyst bed.

The C_3H_8 conversion ($X_{C_3H_8}$), C_3H_6 yield ($Y_{C_3H_6}$) and the selectivity towards each product (S_{Cn}) were estimated as follows:

$$X_{C_3H_8} = \frac{[C_3H_8]_{in}\cdot F_{in} - [C_3H_8]_{out}\cdot F_{out}}{[C_3H_8]_{in}\cdot F_{in}} \times 10 \quad (5)$$

$$Y_{C_3H_6} = (X_{C_3H_8} \bullet S_{C_3H_6})/100 \quad (6)$$

$$S_{C_n} = \frac{[C_n]\cdot n}{[CO] + [CH_4] + 2 \bullet ([C_2H_4] + [C_2H_6]) + 3 \bullet ([C_3H_6])} \times 100 \quad (7)$$

F_{in} and F_{out} referred to the inlet and outlet mole flow rate, $[C_3H_8]_{in}$ and $[C_3H_8]_{out}$ represent the v/v concentrations of C_3H_8 in the inlet and outlet of the reactor, respectively, [CO], $[CH_4]$, $[C_2H_4]$, $[C_2H_6]$ and $[C_3H_6]$ are the v/v concentrations of the generated CO, CH_4, C_2H_4, C_2H_6 and C_3H_6, respectively and n is the number of carbon atoms in each molecule (e.g. 1 for CO and CH_4, 2 for C_2H_4 and C_2H_6, 3 for C_3H_6).

The reaction rate was calculated using the following expression:

$$r_{C_3H_8} = \frac{[C_3H_8]_{in}\bullet F_{in} - [C_3H_8]_{out}\bullet F_{out}}{W} \quad (8)$$

where $r_{C_3H_8}$ is the molar rate of C_3H_8 conversion (mol s^{-1} g_{cat}^{-1}) and W is the mass of catalyst (g_{cat}).

3. Results and discussion

3.1. Catalyst characterization

Results of BET measurements showed that the SSA of Ga_2O_3-TiO_2, Ga_2O_3-Al_2O_3 and Ga_2O_3-SiO_2 catalysts was 47.9, 73.1 and 183.3 m^2 g^{-1}, respectively. The XRD patterns obtained from these catalysts are presented in Fig. 1 where only crystallographic peaks assigned to TiO_2, SiO_2 or Al_2O_3 support were identified indicating that in all cases Ga_2O_3 particles were well dispersed on the support surface [10,25–27]. Specifically, in the case of Ga_2O_3-TiO_2 sample crystallographic peaks at 25.36°, 36.95°, 37.81°, 38.51°, 48.09°, 53.93°, 55.14°, 62.75°, 70.36°, 75.15° and 76.16° were detected which can be attributed to (1 0 1), (1 0 3), (0 0 4), (1 1 2), (2 0 0), (1 0 5), (2 1 1), (2 0 4), (2 2 0), (2 1 5) and (3

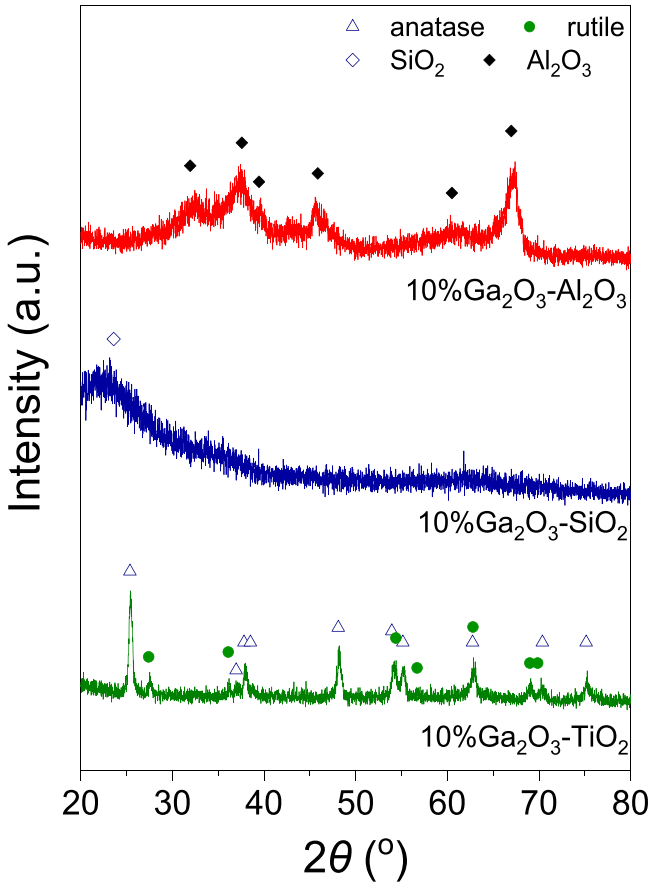

Fig. 1. X-ray diffraction patterns obtained over 10 %Ga_2O_3-TiO_2, 10 %Ga_2O_3-SiO_2 and 10 %Ga_2O_3-Al_2O_3 catalysts.

0 1) planes, respectively, of tetragonal anatase TiO_2 (JCPDS Card No. 4–477), as well as peaks located at 27.42°, 36.09°, 39.21°, 41.28°, 44.15°, 54.38°, 56.70°, 62.80°, 64.11°, 69.0° and 69.86° assigned to (1 1 0), (1 0 1), (2 0 0), (1 1 1), (2 1 0) (2 1 1), (2 2 0), (0 0 2), (3 1 0), (3 0 1) and (1 1 2) planes, respectively, of tetragonal rutile TiO_2 (JCPDS Card No. 21–1276). The anatase content was found equal to 78 % with a primary crystallite size calculated by the Scherrer's equation of 18.3 nm. The crystallite size of rutile phase was found to be lower and equal to 14.9 nm.

The X-ray diffractogram obtained from Ga_2O_3-SiO_2 was characterized by a broad peak located at 23.59° attributed to (2 0 1) reflection of tetragonal SiO_2 (JCPDS Card No. 32–993), while that of Ga_2O_3-Al_2O_3 was characterized by crystallographic peaks detected at 2θ=31.93°, 37.57°, 39.45°, 45.86°, 60.49° and 66.97° corresponding to (2 2 0), (3 1 1), (2 2 2), (4 0 0), (5 1 1) and (4 4 0) planes of cubic Al_2O_3 (JCPDS Card No. 29.63). The primary crystallize size of Al_2O_3 was estimated equal to 6.3 nm, whereas that of SiO_2 couldn't be accurately measured due to the broadness of the single peak detected and its development initiation below 20 ° where no scans were collected.

Supported gallium oxide catalysts were also characterized with respect to their surface basicity employing CO_2-TPD experiments. In these experiments, the as prepared catalysts were treated at 450 °C in He for 15 min. Pretreatment conditions were selected based on our previous tests which showed that any adsorbed surface species can be easily removed from the catalyst surface by heating it at 450 °C. The catalyst was then cooled followed by 1 % CO_2/He adsorption at 25 °C for 30 min and subsequently, 30 minutes purging with He. The TPD was then initiated using a heating rate of 10 °C/min and a total flow rate of 30 cm^3 min^{-1}. The CO_2-TPD profiles are presented in Fig. 2 where it is observed that in the case of Ga_2O_3-SiO_2 catalyst two CO_2 desorption regions were detected; a low-temperature (LT) region where a weak peak centered at 77 °C can be discerned and a high-temperature (HT) region above 500 °C where more than one peaks of significantly higher intensity were evolved which were present up to 750 °C, at which point the TPD was stopped. The LT peak was previously assigned to CO_2 desorption from weak basic sites while the HT features were attributed to CO_2 desorption from medium and/or strong basic sites [28–32].

Qualitatively similar results were obtained over Ga_2O_3-Al_2O_3 and Ga_2O_3-TiO_2 catalysts (Fig. 2) which, however, exhibited the following differences: both the HT and, especially, the LT desorption peak increased in intensity, with the former started evolving at lower temperatures (above 410 °C for Ga_2O_3-Al_2O_3 and above 350 °C for Ga_2O_3-TiO_2). The amount of CO_2 desorbed (in μmol g^{-1}) from the weak and medium/strong basic sites was calculated by integrating the area below the LT and HT peak, respectively (Table S1). To eliminate the factor attributed to the SSA which was significantly varied (from 47.9 to 183.3 m^2 g^{-1}), the estimated values of desorbed CO_2 were normalized with respect to the SSA and results obtained (in μmol m^{-2}) are presented in Table 1. It was found that the amount of CO_2 desorbed in the LT region increased from 0.002 to 0.313 μmol m^{-2} in the order Ga_2O_3-SiO_2 < Ga_2O_3-TiO_2 < Ga_2O_3-Al_2O_3. Although the amount of CO_2 desorbed in the HT region was also lower for Ga_2O_3-SiO_2 catalyst (0.022 μmol m^{-2}), it was found to be higher for Ga_2O_3-TiO_2 (0.305 μmol m^{-2}) than for Ga_2O_3-Al_2O_3 (0.233 μmol m^{-2}). Results provide evidence that the number of weak basic sites was higher over Ga_2O_3-Al_2O_3 catalyst compared to Ga_2O_3-TiO_2 while the opposite occurred for medium/strong basic sites. The lowest number of both weak and medium/strong basic sites was observed for Ga_2O_3-SiO_2 catalyst. The total amount of desorbed CO_2 and therefore, the total surface basicity, was estimated by integrating the total area below the CO_2 response curve and was found to increase in the order Ga_2O_3-SiO_2 (0.024 μmol m^{-2}) < Ga_2O_3-Al_2O_3 (0.546 μmol m^{-2}) < Ga_2O_3-TiO_2 (0.582 μmol m^{-2}).

Qualitatively, similar results were obtained over bare TiO_2 (36.9 m^2/g), Al_2O_3 (95.7 m^2/g) and SiO_2 (222.1 m^2/g) supports (Fig.S2, Table 1 and S1). Comparison with the corresponding results obtained over the Ga_2O_3 containing samples (Fig. 2, Table 1) showed that the intensity of both peaks and thereby, the total amount of desorbed CO_2 were significantly lower for bare supports, indicating that the surface basicity was improved with the addition of Ga_2O_3, which, however, followed the same trend with respect to the nature of the support.

The surface basicity of Ga_2O_3 based catalysts was also examined by Xu et al. [8], who found that the number of basic sites on the catalyst surface increased following the order Ga_2O_3-SiO_2 << Ga_2O_3-TiO_2 < Ga_2O_3-Al_2O_3. Similarly, Petre et al. [33] demonstrated that the CO_2 uptake was higher over Ga_2O_3-Al_2O_3 followed by Ga_2O_3-TiO_2 and Ga_2O_3-SiO_2 catalysts which both exhibited very weak basicity. The increase of surface basicity by gallium oxide deposition on alumina surface was also reported by Michorczyk et al. [34]. According to these authors, an increase of Ga_2O_3 loading resulted in an increase of the selectivity of products formed on basic sites for two tests reactions (conversion of isopropanol and conversion of 2-methyl-3-butyn-2-ol), suggesting an increase of the overall surface basicity. The small differences observed between the catalysts' ranking with respect to their basicity reported in literature and the results of the present study can be attributed to the different commercial metal oxide powders used as supports and/or the different method applied for catalysts synthesis.

Similar experiments were conducted by in situ DRIFTS over the synthesized catalysts where the following procedure was employed: heating in He flow at 450 °C for 15 min → cooling at 25 °C in He flow → switch of the flow to 5 %CO_2/He for 30 min→ purging with He for 30 min → DRIFT spectrum collection at 25 °C → stepwise increase of

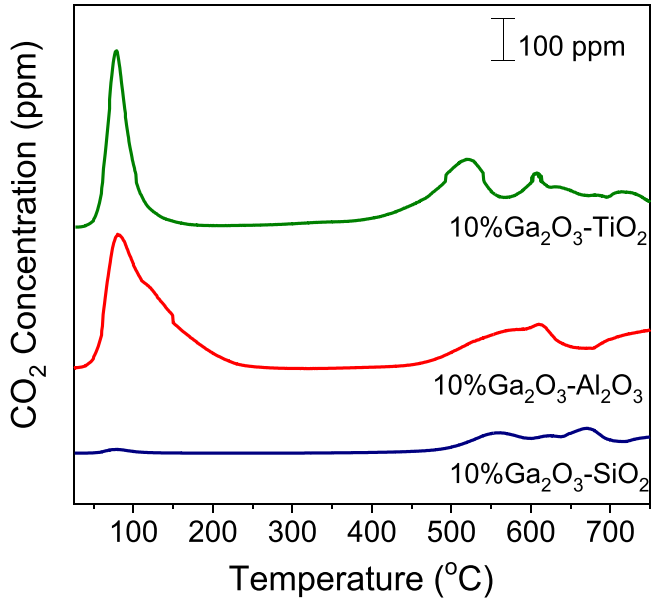

Fig. 2. CO_2-TPD profiles obtained from 10 %Ga_2O_3-SiO_2, 10 %Ga_2O_3-Al_2O_3 and 10 %Ga_2O_3-TiO_2 catalysts. Experimental conditions: Mass of catalyst: 0.15 g; particle diameter: 0.15 <d_p < 0.25 mm; heating rate β=10 °C/min; total flow = 30 cm^3 min^{-1}.

Table 1
Total amount of desorbed CO_2 during CO_2-TPD experiments.

Catalyst	LT peak (μmol·m^{-2})	HT peak (μmol·m^{-2})	Total amount of desorbed CO_2 (μmol·m^{-2})
10 %Ga_2O_3-SiO_2	0.002	0.022	0.024
10 %Ga_2O_3-TiO_2	0.278	0.305	0.582
10 %Ga_2O_3-Al_2O_3	0.313	0.233	0.546
SiO_2	0.001	0.007	0.008
TiO_2	0.111	0.055	0.166
Al_2O_3	0.126	0.034	0.160

temperature up to 450 °C during which DRIFT spectra were collected at selected temperatures after an equilibration time of 3 min. It should be clarified that, besides the times of CO_2 adsorption and purging with He, which were the same, the reaction conditions used in CO_2-TPD experiments were different than those used in DRIFTS studies (e.g. reactor type/operation, mass of catalyst, CO_2 concentration etc.). Results of DRIFTS experiments can only be used to extract information related to the nature and relative variation of adsorbed surface species with temperature, and can only be qualitatively compared with those obtained by Mass Spectrometry studies (Fig. 2), which are able to quantitively identify the number and strength of basic sites on the catalyst surface.

Results obtained over Ga_2O_3-SiO_2 catalyst are presented in Fig. 3A. The spectrum recorded at 25 °C (trace a) was characterized by a single weak band located at 1629 cm^{-1} previously assigned to bicarbonate (HCO_3^-) species associated with Ga_2O_3 surface [35–37]. The intensity of this band decreased with increasing temperature and disappeared above 150–200 °C implying that CO_2 was weakly adsorbed on the surface of Ga_2O_3-SiO_2 catalyst most possibly due to the acidic character of SiO_2 support in agreement with previous studies [38,39].

Fig. 3B shows the corresponding DRIFT spectra obtained from Ga_2O_3-TiO_2 catalyst following CO_2 adsorption. As it can be seen, the spectrum recorded at 25 °C (trace a) consisted of two bands at 1649 and 1416 cm^{-1} previously attributed to bicarbonate species and two bands at 1580 and 1320 cm^{-1} due to bidentate carbonates adsorbed on TiO_2 [40–44] and/or Ga_2O_3 [35–37] surface. Increase of temperature at 150 °C resulted in the development of a band at 1538 cm^{-1} which can be attributed to monodentate carbonate species associated with TiO_2 [40–42,44,45] and may be pre-existed at lower temperatures but couldn't be distinct due to overlapping with the broad band at 1649 cm^{-1}. Although the intensity of all bands decreased with further increase of temperature, they did not disappear even at 450 °C (trace i) indicating that the corresponding surface species were strongly adsorbed on the catalyst surface.

The adsorption of CO_2 on Ga_2O_3-Al_2O_3 surface led to the formation of similar surface species with those discussed above over Ga_2O_3-TiO_2 (Fig. 3C). Particularly, bands due to bicarbonates (1642 and 1402 cm^{-1}), monodentate and bidentate carbonates (1521, 1557 and 1361 cm^{-1}) were detected on the spectrum obtained at 25 °C [35,37, 46–50]. The relative population of surface species decreased upon heating the catalyst under He flow and was eliminated above 300 °C (trace f) indicating their desorption from the catalyst surface. Results of Fig. 3 imply that the adsorption strength of CO_2 was enhanced following the order Ga_2O_3-SiO_2 < Ga_2O_3-Al_2O_3 < Ga_2O_3-TiO_2 in excellent agreement with CO_2-TPD results of Fig. 2.

Regarding the structure of basic sites, two general types of basic sites have been suggested to be present on metal oxides, namely surface hydroxyl groups (weak Brønsted basic sites) and low-coordination oxygen anions (strong basic sites) [51,52]. Previous studies demonstrated that CO_2 is preferentially adsorbed on these sites leading to the formation of bicarbonate species (via its interaction with OH groups) and bidentate, monodentate and/or bridged carbonate species (via its interaction with oxygen anions) [46,49–51,53,54] in accordance to the results of Fig. 3. Aziz et al. [52] stated that the former species are desorbed from the catalyst surface at low temperatures contributing to the low temperature CO_2 evolution in the CO_2-TPD profiles, while the latter species are responsible for the CO_2 peaks evolved at high temperatures. Basic sites of medium strength may be also present on the catalyst surface contributing to CO_2 desorption at medium temperatures during CO_2-TPD experiments [52]. Therefore, concerning the results of Figs. 2 and 3, it can be suggested that, in the case of titania and alumina supported catalysts, the LT peak in the CO_2-TPD profile was due to desorption of bicarbonate species formed via interaction of CO_2 with basic hydroxyl groups and the HT peak to desorption of bidentate and monodentate carbonate species generated by interaction of CO_2 with basic surface oxygen species. However, in the case of silica supported catalyst, the interaction of which with CO_2 led to the development of a single weak peak due to bicarbonates, the CO_2 release both in the low and high temperature region seems to be due to decomposition of these

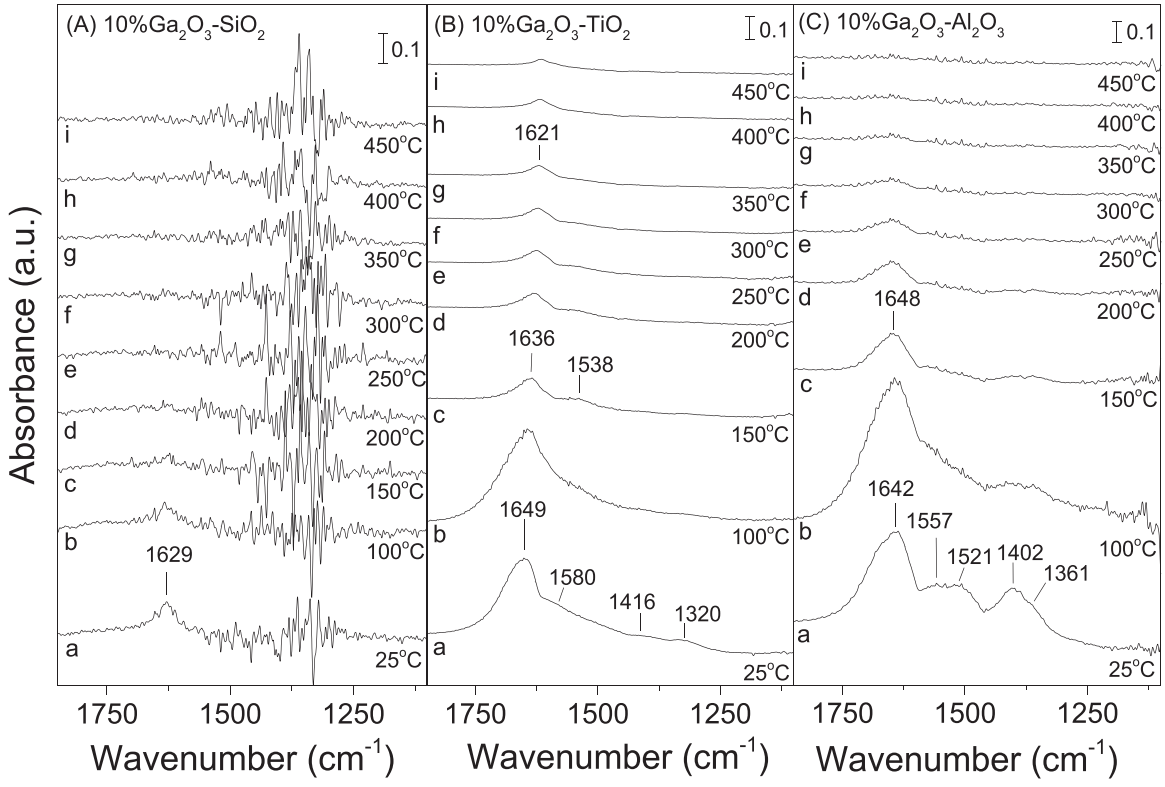

Fig. 3. DRIFT spectra obtained from (A) 10 %Ga_2O_3-SiO_2, (B) 10 %Ga_2O_3-TiO_2 and (C) 10 %Ga_2O_3-Al_2O_3 catalysts following adsorption of CO_2 at 25 °C for 30 min and subsequent stepwise heating at the indicated temperatures under He flow.

species.

The acidity of the investigated catalysts was probed by TGA experiments following NH_3 adsorption at 25 °C [1]. The corresponding weight loss (%) and TGA derivative curves as a function of temperature are depicted in Fig. 4 and S2. It was observed that all catalysts exhibited three weight loss regions centered at ~200–280 °C, 350–420 °C and 480–530 °C assigned to weak, moderate and strong acid sites, respectively [27,55–60]. Any weight loss observed at temperatures lower than 120 °C was possibly due to removal of residual physisorbed water [61]. The weight loss was found to be higher for the Ga_2O_3-SiO_2 catalyst followed by Ga_2O_3-Al_2O_3 and then Ga_2O_3-TiO_2 (Fig. 4). The acid sites density was calculated following the procedure described in the Supplementary Material [1] and results are presented in Table S2. As it can be seen the total surface acidity was found to be 673.5 μmol·g^{-1} for Ga_2O_3-TiO_2, 1082.1 μmol·g^{-1} for Ga_2O_3-Al_2O_3 and 1548.3 μmol·g^{-1} for Ga_2O_3-SiO_2 implying that the silica supported catalyst was characterized by the highest number of acid sites per gram of catalyst while the titania supported catalyst was the least acidic one. Comparison of these values with the SSA of the investigated catalysts showed that the acid site density per gram of catalyst increases monotonically with increasing the SSA. Therefore, if the aforementioned values are expressed per unit surface area, the catalysts ranking with respect to the density of surface acid sites is modified as follows: Ga_2O_3-SiO_2 (8.45 μmol·m^{-2}) < Ga_2O_3-TiO_2 (14.07 μmol·m^{-2}) < Ga_2O_3-Al_2O_3 (14.80 μmol·m^{-2}) (Table 2). Results are in agreement with those reported by Shao et al. [60], who found that Ga_2O_3-Al_2O_3 catalyst exhibited higher total acidity, estimated by NH_3-TPD experiments, compared to Ga_2O_3-SiO_2. Similar experiments were conducted by Xu et al. [8] who found that the number of medium to strong acid sites increased in the sequence Ga_2O_3-SiO_2 < Ga_2O_3-TiO_2 < Ga_2O_3-Al_2O_3. Similarly, Petre et al. [33] demonstrated that the number of acid sites measured by pyridine adsorption increased in the order Ga_2O_3-SiO_2 < Ga_2O_3-TiO_2 < Ga_2O_3-Al_2O_3, which was correlated with the degree of Ga_2O_3 dispersion as well as the Ga_2O_3-support interactions. In addition, Shen at al. [56] reported that the acidity of Ga_2O_3/HZSM-5 catalyst decreased with increasing the Si/Al ratio of the support.

Similar TGA experiments following NH_3 adsorption were carried out over bare TiO_2, Al_2O_3 and SiO_2 supports and results obtained showed that, in all cases, the surface acidity was lower compared to that measured for Ga_2O_3-M_xO_y catalysts (Fig.S3). The total acid site density was found to increase following the order SiO_2 (4.42 μmol·m^{-2}) < TiO_2 (8.44 μmol·m^{-2}) < Al_2O_3 (11.97 μmol·m^{-2}) which was the same with that found in the presence of Ga_2O_3 (Table 2). Results imply that surface acidity was enhanced by Ga_2O_3 addition in agreement with our previous study [1].

Table 2
Acid site density estimated from TGA experiments over 10 %Ga_2O_3-SiO_2, 10 % Ga_2O_3-TiO_2 and 10 %Ga_2O_3-Al_2O_3.

Catalyst	Acid Site Density (μmol·m^{-2})			
	Weak	Moderate	Strong	Total
10 % Ga_2O_3-SiO_2	3.76	3.41	1.28	8.45
10 % Ga_2O_3-TiO_2	5.48	5.35	3.24	14.07
10 %Ga_2O_3-Al_2O_3	7.32	4.69	2.78	14.80
SiO_2	-	2.78	1.64	4.42
TiO_2	3.82	4.62	-	8.44
Al_2O_3	7.61	3.07	1.29	11.97

The nature of acid sites on the catalyst surface was determined by adsorption of pyridine coupled with FTIR spectroscopy and results obtained over Ga_2O_3-M_yO_y are presented in Fig. 5. The spectrum recorded for Ga_2O_3-SiO_2 catalyst was characterized by four characteristic peaks located at 1622, 1492, 1458 and 1598 cm^{-1} assigned to pyridine adsorption on Lewis acid sites as well as by two bands detected at 1640 and 1549 cm^{-1} due to pyridine protonated by strong Brønsted acid sites [62–65]. The band at 1492 cm^{-1} may also contain contribution from pyridine adsorption on Brønsted acid sites [62,65]. A weak peak at 1578 cm^{-1} and a shoulder at 1446 cm^{-1} were also observed which can be attributed to physisorbed pyridine [62–64]. It should be noted that the bands at 1622 and 1458 cm^{-1} were previously associated with strong Lewis acid sites, while that at 1598 cm^{-1} with moderate and weak Lewis acid sites indicating the presence of different strength of acid sites on the catalyst surface in agreement with the results of Fig. 4 and S2 [64,66,67].

The spectra collected for Ga_2O_3-Al_2O_3 catalyst (Fig. 5) consisted of

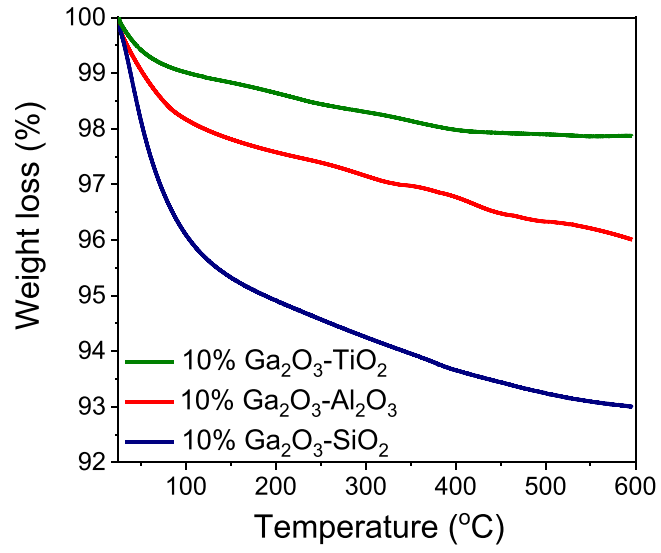

Fig. 4. TGA curves following NH_3 adsorption at 25 °C obtained from the 10 % Ga_2O_3-SiO_2, 10 %Ga_2O_3-Al_2O_3 and 10 %Ga_2O_3-TiO_2 catalysts.

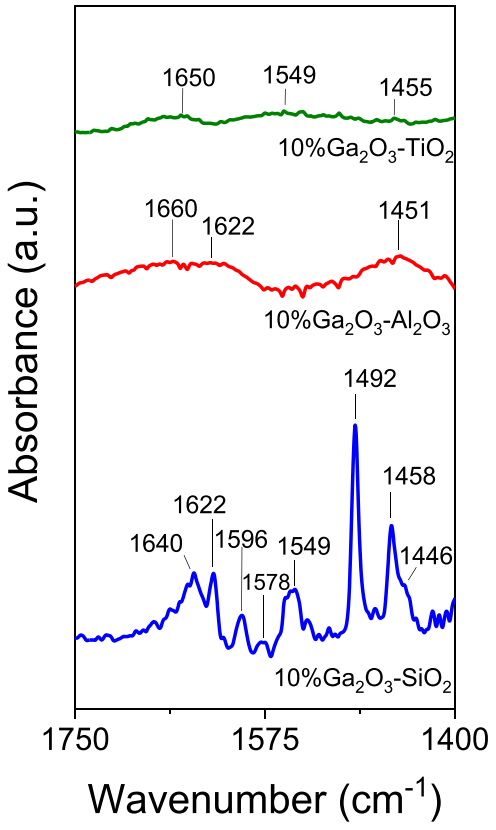

Fig. 5. DRIFT spectra obtained following pyridine adsorption at 25 °C over 10 %Ga_2O_3-SiO_2, 10 %Ga_2O_3-Al_2O_3 and 10 %Ga_2O_3-TiO_2 catalysts.

two broad bands related to the interaction of adsorbed pyridine species with Lewis acid sites (1622 and 1452 cm^{-1}) [13,67–69] and a broad band at 1660 cm^{-1} which, although was appeared at higher wavenumbers, may contain contribution from pyridine species adsorbed on Brønsted acid sites. However, no band was observed in the 1540–1550 cm^{-1} region assigned to pyridinium anions, implying that the number/strength of Brønsted acid sites was low in order to protonate the adsorbed pyridine in agreement with previous studies over Ga_2O_3-Al_2O_3 catalysts [13,68]. It should be also mentioned that more than one overlapping peaks may coexist in the three detected regions, which cannot be clearly distinguished in the obtained spectra due to the broadness of the detected bands. This was also the case for Ga_2O_3-TiO_2 catalyst, the interaction of which with pyridine gave rise to the development of two broad bands at 1650 and 1558 cm^{-1} attributed to protonated pyridine on Brønsted acid sites and a weak peak at 1455 cm^{-1} most possibly due pyridine coordinated with Lewis acid sites in agreement with previous studies over titania based catalysts [70–72].

Temperature programmed reduction experiments using H_2 as the reducing agent were also carried out using the following procedure: heating in He flow at 450 °C for 15 min → oxidation at 300 °C under 20.5 % O_2/He flow (30 cm^3 min^{-1}) → heating in He flow at 450 °C for 15 min → cooling at 25 °C in He flow → switch of the flow to 3 %H_2/He → increase of temperature up to 750 °C using a rate of 10 °C min^{-1}. Results (Fig.S4) showed that no reduction peaks were observed in the H_2-TPR profiles of Ga_2O_3-SiO_2 and Ga_2O_3-Al_2O_3 catalysts implying that reduction of these catalysts by hydrogen was limited (at least below 750 °C) in agreement with previous studies [8,60]. In contrast, the H_2-TPR profile obtained from the Ga_2O_3-TiO_2 catalyst was characterized by two hydrogen consumption peaks located at 338 °C and 598 °C. The former peak can be attributed to the reduction of well dispersed Ga species and/or GaO^+ species interacting with the support, while the latter peak can be assigned to reduction of bulk or larger Ga_2O_3 particles [1,60,73,74]. It should be noted that the high temperature peak may also contain contributions from the reduction of the TiO_2 surface [1,75,76]. The total amount of H_2 consumed estimated by the area below the H_2 response curve of Ga_2O_3-TiO_2 catalyst was found equal to 106.5 μmol g^{-1}. Based on our recent study, the reducibility of TiO_2 was significantly enhanced with the addition of Ga_2O_3 on TiO_2 surface with the amount of consumed hydrogen being increased by a factor of 3.5 [1]. The inability of hydrogen consumption by Ga_2O_3-SiO_2 and Ga_2O_3-Al_2O_3 catalysts may be related to the well-known "irreducible" character of SiO_2 and Al_2O_3 supports which prevents stabilization of small gallium oxide particles or GaO^+ [60].

3.2. Effect of the support nature on catalytic performance

The effect of the nature of the oxide carrier (SiO_2, TiO_2, Al_2O_3) on the catalytic performance of supported 10 wt% Ga_2O_3 catalysts for the CO_2-ODP reaction was investigated and results obtained are presented in Fig. 6. The selection of Ga_2O_3 content was based on preliminary experiments conducted over x%Ga_2O_3-Al_2O_3 catalysts which showed that both X_{C3H8} and S_{C3H6} were progressively increased with increasing Ga_2O_3 loading while side products formation was suppressed as the Ga_2O_3 content increased up to 10 wt% (Fig.S5). Although higher propane conversions can be achieved with further increase of Ga_2O_3 loading to 20 wt%, selectivities towards all reaction products remained constant providing evidence that 10 wt% of Ga_2O_3 was a suitable content, which may also ensure a better dispersion of gallium oxide particles compared to that of 20 wt%. It was found that Ga_2O_3-SiO_2 and Ga_2O_3-TiO_2 catalysts were both activated above 570 °C and reached $X_{C_3H_8}$=80 % at 745 °C (Fig. 6A). Alumina supported Ga_2O_3 catalyst exhibited higher catalytic activity below 700 °C giving measurable propane conversions at temperatures higher than 510 °C. However, $X_{C_3H_8}$ at 745 °C was found to be equal (80 %) to that measured for Ga_2O_3-SiO_2 and Ga_2O_3-TiO_2 catalysts. The effect of the support nature on propylene yield was more pronounced and be dependent on the reaction temperature (Fig. 6B). Specifically, below 650 °C the $Y_{C_3H_6}$ increased in the order Ga_2O_3-TiO_2 (5.4 % at 600 °C) < Ga_2O_3-SiO_2 (7.8 % at 600 °C) < Ga_2O_3-Al_2O_3 (18.7 % at 600 °C), whereas higher reaction temperatures had a negative effect on propylene yield of Ga_2O_3-Al_2O_3 catalyst. In particular, the $Y_{C_3H_6}$ for this sample presented a maximum value around 600 °C and then decreased with further increase of temperature contrary to the $Y_{C_3H_6}$ measured for Ga_2O_3-TiO_2 and Ga_2O_3-SiO_2 catalysts which was gradually increased with increasing temperature.

In addition to propylene, the products detected under reaction conditions were CO, CH_4, C_2H_4 and traces of C_2H_6. The effect of reaction temperature on products selectivity for the investigated catalysts is presented in Fig. 7. As it can be seen, propylene selectivity ($S_{C_3H_6}$) measured for Ga_2O_3-SiO_2 catalyst decreased from 69 % to 23 % with increasing temperature from 590 to 745 °C, whereas CO selectivity (S_{CO}) remained almost stable in the entire temperature range examined fluctuating between 13 % and 19 % (Fig. 7A). The selectivity towards C_2H_4 ($S_{C_2H_4}$) and CH_4 (S_{CH_4}) progressively increased from 8 % to 36 % and from 4.5 % to 22 %, respectively, with increasing temperature in the range of 590–745 °C, whereas that of C_2H_6 ($S_{C_2H_6}$) was not exceeded 1.2 % in the entire temperature range examined. The production of both C_3H_6 and CO provides evidence that the desired CO_2-assisted ODP reaction was taking place. However, the decrease of $S_{C_3H_6}$ with

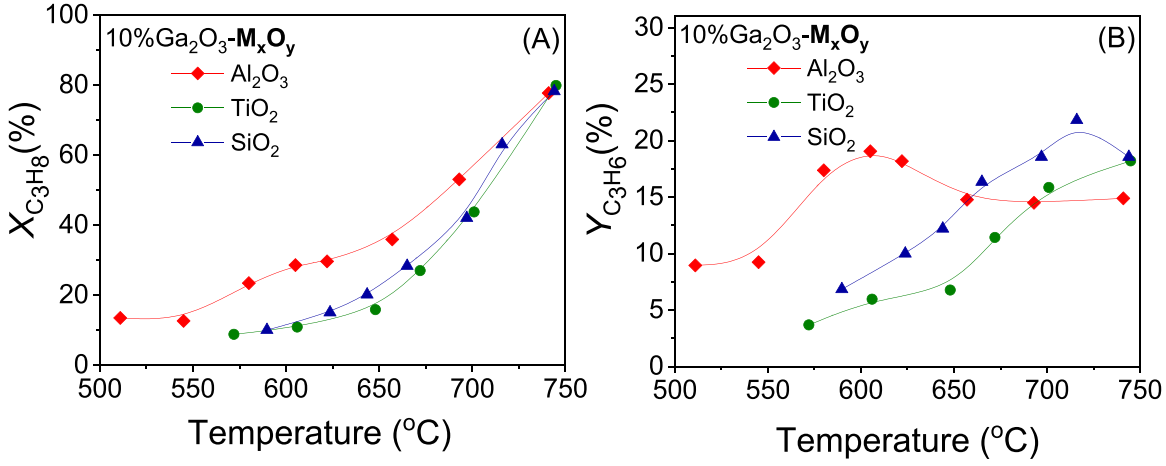

Fig. 6. Effect of reaction temperature on the (A) conversion of C_3H_8 and (B) C_3H_6 yield obtained over 10 %Ga_2O_3-TiO_2, 10 %Ga_2O_3-SiO_2 and 10 %Ga_2O_3-Al_2O_3 catalysts. Experimental conditions: Mass of catalyst: 0.5 g; particle diameter: 0.15 <d_p < 0.25 mm; Feed composition: 5 % C_3H_8, 25 % CO_2 (balance He); Total flow rate: 50 cm^3 min^{-1}.

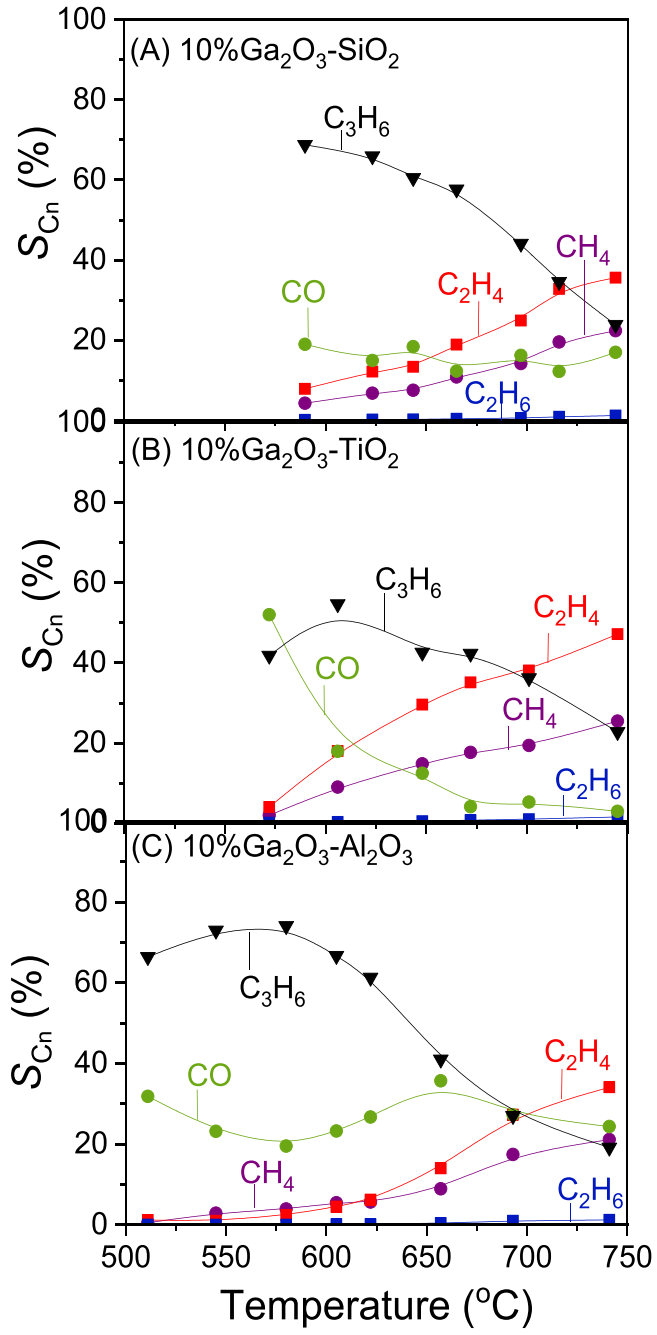

Fig. 7. Selectivities towards reaction products as a function of temperature obtained over (A) 10 %Ga_2O_3-SiO_2, (B) 10 %Ga_2O_3-TiO_2 and (C) 10 %Ga_2O_3-Al_2O_3 catalysts. Experimental conditions: same as in Fig. 6.

temperature in combination with the progressive increase of both $S_{C_2H_4}$ and S_{CH_4} indicates that propane or propylene decomposition (9−12) as well as propane hydrogenolysis (13, 14) may run in parallel hindering further production of propylene. The occurrence of reaction (9) may also be responsible for the almost stable selectivity towards CO which was expected to be decreased under conditions where CO_2-ODP (3) reaction was suppressed. In addition, production of CO may also take place via the reverse Boudouard reaction (15).

$$2CO_2 + 2C_3H_8 \leftrightarrow 3C_2H_4 + 2CO + 2H_2O \qquad \Delta H^0_{298K} = 447.2\ \text{kJ/mol} \tag{9}$$

$$C_3H_8 \leftrightarrow C_2H_4 + CH_4 \qquad \Delta H^0_{298K} = 81.7\ \text{kJ/mol} \tag{10}$$

$$2C_3H_6 \leftrightarrow 2CH_4 + C_2H_4 + 2C(s) \qquad \Delta H^0_{298K} = -137.6\ \text{kJ/mol} \tag{11}$$

$$C_3H_8 \leftrightarrow CH_4 + 2H_2 + 2C(s) \qquad \Delta H^0_{298K} = 29.2\ \text{kJ/mol} \tag{12}$$

$$C_3H_8 + H_2 \leftrightarrow C_2H_6 + CH_4 \qquad \Delta H^0_{298K} = -55.4\ \text{kJ/mol} \tag{13}$$

$$C_3H_8 + 2H_2 \leftrightarrow 3CH_4 \qquad \Delta H^0_{298K} = -120.0\ \text{kJ/mol} \tag{14}$$

$$CO_2 + C \leftrightarrow 2CO \qquad \Delta H^0_{298K} = 172.4\ \text{kJ/mol} \tag{15}$$

The same products were detected over Ga_2O_3-TiO_2 (Fig. 7B) and Ga_2O_3-Al_2O_3 (Fig. 7C) catalysts. Comparison of the results obtained with those discussed above over Ga_2O_3-SiO_2 (Fig. 7A) showed the following differences: (a) $S_{C_3H_6}$ was lower in the whole temperature range examined over Ga_2O_3-TiO_2 (e.g. $S_{C_3H_6}$ =50 % at 600 °C) contrary to Ga_2O_3-Al_2O_3 and Ga_2O_3-SiO_2 which exhibited comparable selectivities towards propylene (e.g. $S_{C_3H_6}$ =68 % at 600 °C); (b) S_{CO} was significantly higher at low reaction temperatures and progressively decreased (from 52 % to 3 %) with temperature for Ga_2O_3-TiO_2, indicating that the reactions leading to CO production were favored at low temperatures and suppressed above 670 °C. On the other hand, S_{CO} measured over Ga_2O_3-Al_2O_3 decreased slightly with temperature below 580 °C and then increased again exhibiting a maximum value of 36 % at ~660 °C; (c) Silica- and alumina-supported catalysts exhibited similar values of $S_{C_2H_4}$ and S_{CH_4} at a given temperature which were found to be lower compared to those measured for titania-supported sample, implying that the side reactions of propane or propylene decomposition (9−12) and propane hydrogenolysis (13, 14) were facilitated over Ga_2O_3-TiO_2

catalyst. Interestingly, the production of undesired C_2H_4 and CH_4 over the most active Ga_2O_3-Al_2O_3 catalyst was limited below 600 °C where propylene yield presented its maximum values, indicating that C_3H_8 was mainly converted to C_3H_6 and CO via CO_2-ODP reaction at temperatures of practical interest.

Concerning the physicochemical properties of catalysts discussed above a general trend was observed according to which catalytic performance is strongly correlated with the amount of CO_2 desorbed during CO_2-TPD experiments (Fig. 2, Table 1). As it can be seen in Fig. 8A, propane conversion, propylene yield and reaction rate normalized with respect to the SSA ($r_{C3H8,}$ in μmol m^{-2}) measured at 600 °C were optimized for the Ga_2O_3-Al_2O_3 catalyst characterized by a moderate surface basicity. This is in agreement with results of our previous study over titania based composite metal oxides (M_xO_y-TiO_2, M: Ce, Zr, Ca, Cr, Ga) where a moderate surface basicity was found to be crucial for the activation of CO_2 and thus, the efficient conversion of propane towards propylene via CO_2-ODP reaction [1].

Regarding surface acidity, a similar diagram of $X_{C_3H_8}$, $Y_{C_3H_6}$ and r_{C3H8} measured at 600 °C as a function of the acid site density estimated by TGA experiments (Fig. 4) was plotted (Fig. 8B). No monotonous trend of $X_{C_3H_8}$ and $Y_{C_3H_6}$ was observed with respect to surface acidity expressed in μmol m^{-2}. The most acidic Ga_2O_3-Al_2O_3 catalyst was found to be superior in activity for the CO_2-ODP reaction whereas the least acidic Ga_2O_3-SiO_2 catalyst exhibited intermediate performance which was slightly improved compared to Ga_2O_3-TiO_2 characterized by moderate acidity. However, a clearer trend was observed by correlating the normalized reaction rate with the acid site density, according to which r_{C3H8} increased by one order of magnitude with increasing the surface acidity, following the order Ga_2O_3-SiO_2 < Ga_2O_3-TiO_2 < Ga_2O_3-Al_2O_3.

Based on the above, it is evident that the observed catalyst ranking with respect to ODP activity is strongly related to the catalysts' acid/base properties. A high surface acidity and a moderate surface basicity seem to be desirable in order to achieve high rates of propane conversion towards propylene at temperatures of practical interest (<650 °C).

The effect of the support nature for the CO_2-assisted propane dehydrogenation over supported Ga_2O_3 catalysts was also investigated by Xu et al. [8], who found that propane conversion decreased in the order

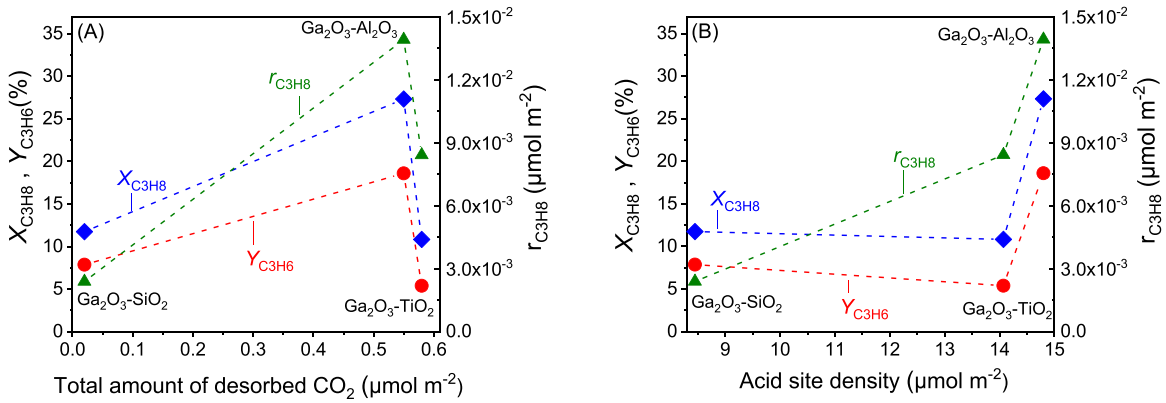

Fig. 8. Propane conversion, propylene yield and normalized reaction rate per unit surface area obtained at 600 °C as a function of (A) the total amount of CO_2 desorbed during CO_2-TPD experiments and (B) the surface acidity estimated by TGA following NH_3 adsorption over the supported Ga_2O_3 catalysts.

Ga_2O_3/TiO_2 > Ga_2O_3/ZrO_2 > Ga_2O_3/Al_2O_3 > Ga_2O_3/SiO_2 > Ga_2O_3/MgO. According to the authors the interactions between the gallium oxide and the support caused variations in H_2 adsorption capacities and acid-base properties which were found to be responsible for the observed differences in catalytic activity as well as for the observed different support effects on the promoting or not role of CO_2 on propylene production. The higher catalytic activity of alumina- compared to silica-supported gallium oxide was also demonstrated by Zhou et al. [20]. Similarly, Xiao et al. [15] found that when the Ga_2O_3-Al_2O_3 catalyst was prepared by the hydrothermal synthesis method it was able to achieve propane conversion of 35.2 % and propylene selectivity of 95 % at temperatures as low as 550 °C. This was attributed to the high surface area (234 m^2 g^{-1}) of this catalyst and the higher amount of tetrahedral Ga ions correlated with the medium-strong Lewis acid sites. Moreover, Shao et al. [60] reported that when gallium oxide was dispersed on alumina support, a higher initial propane conversion of 46 % was achieved at 620 °C compared to the case that it was dispersed on silica which resulted in a low propane conversion of 5.5 % for the propane dehydrogenation reaction. According to these authors the weak interactions between Ga species and SiO_2 support in combination with the limited reducibility and the low amount of well-dispersed Ga species observed for Ga_2O_3-SiO_2 catalyst were responsible for its lower catalytic activity.

Regarding results of the present study, a synergistic interaction be-

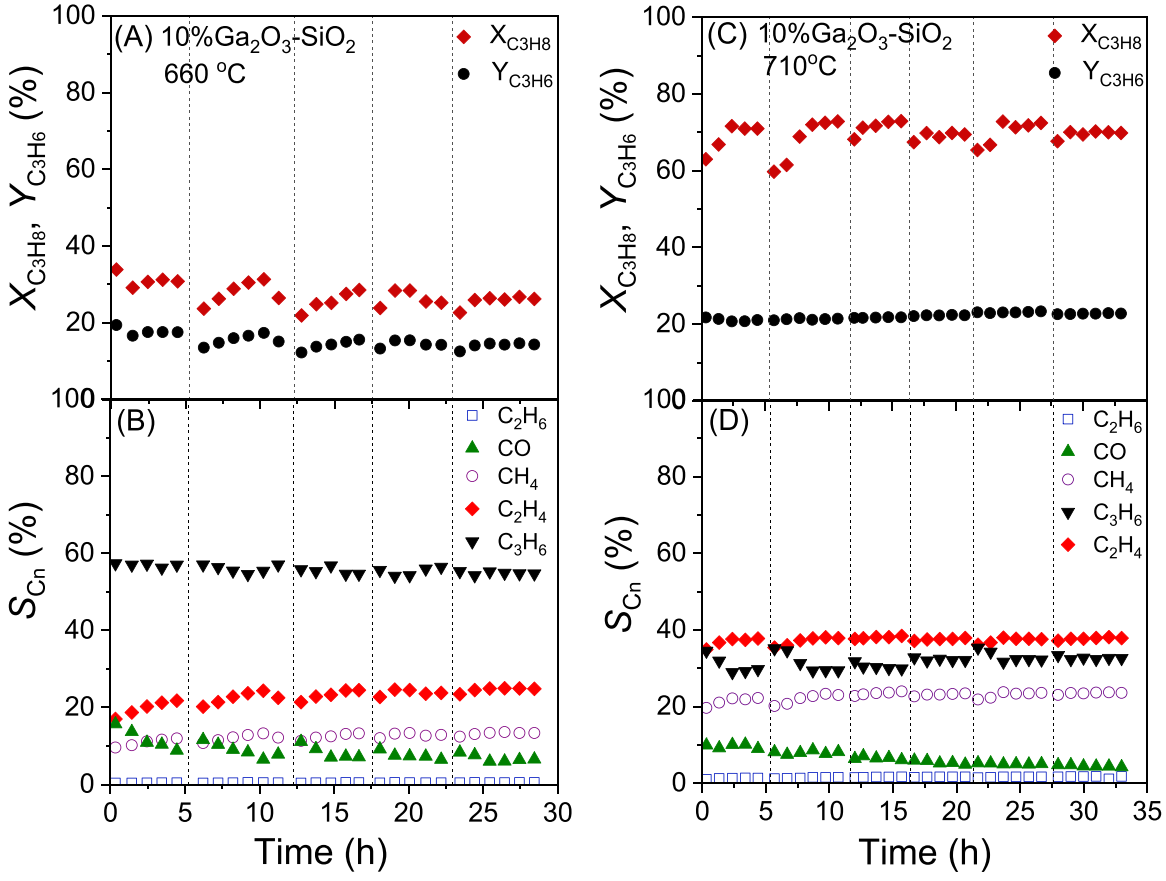

Fig. 9. TOS stability test of the 10 %Ga_2O_3-SiO_2 catalyst conducted at (A, B) 660 °C and (C, D) 710 °C under conditions of oxidative dehydrogenation of C_3H_8 with CO_2. Alterations of (A, C) $X_{C_3H_8}$ and $Y_{C_3H_6}$, and (B, D) products selectivity with time-on-stream. Experimental conditions: Same as in Fig. 5. Dashed vertical black lines indicate shutting down of the system overnight where the catalyst remained under He flow.

tween gallium oxide particles and the support employed seems to be occurred in all cases examined as evidenced by the improved catalytic performance of the supported Ga_2O_3 catalysts compared to that of the bare Ga_2O_3 and the corresponding bare support (Fig.S6). This synergy was found to be enhanced when alumina was used as support as $X_{C_3H_8}$ at 600 °C increased from ~3–4 % for bare Al_2O_3 and Ga_2O_3 to 29 % for Ga_2O_3-Al_2O_3 (Fig.S6E). This was also the case for $Y_{C_3H_6}$ which was found to be 19-fold higher for Ga_2O_3-Al_2O_3 than that measured for the corresponding bare metal oxides (Fig.S6F).

3.3. Time-on-stream (TOS) stability tests

The time on stream stability of Ga_2O_3-SiO_2 catalyst for the CO_2-ODP reaction was investigated at 660 and 710 °C and results obtained are presented in Fig. 9. It was observed that $X_{C_3H_8}$ and $Y_{C_3H_6}$ measured at 660 °C were varied in the ranges of 30–34 % and 16.6–19.4 %, respectively, during the first five hours on stream (Fig. 9A). The measurements obtained following shutting down of the system overnight and remaining in He flow showed that both $X_{C_3H_8}$ and $Y_{C_3H_6}$ were slightly lower. However, they both increased with time regaining their initial values and then were slightly decreased again until the next shutting down of the system. This indicates that Ga_2O_3-SiO_2 catalyst loose part of its initial activity during shutting down of the system which can be, however, retrieved with subsequent catalyst exposure to the reaction mixture. The same trend was observed with further increase of time which was, however, smoothed out after 17 hours on stream leading to stabilization of both $X_{C_3H_8}$ and $Y_{C_3H_6}$ at 26 and 14.5 %, respectively. Results of products distribution (Fig. 9B) showed that $S_{C_3H_6}$ was almost stable (54.5–57 %) during the entire stability test contrary to S_{CO} which exhibited a small decrease after each shutting down of the system during the night. On the other hand, $S_{C_2H_4}$ and S_{CH_4} were gradually increased from 17 % to 24.5 % and from 9.6 % to 13.4 %, respectively, after 30 hours on stream, while $S_{C_2H_6}$ was always lower than 0.5 %.

Qualitatively similar results were obtained at 710 °C with $X_{C_3H_8}$, $Y_{C_3H_6}$ and S_{Cn} exhibiting the same trends with those observed at 660 °C. As it was expected, propane conversion (60–72 %) and propylene yield (21–23 %) were higher at 710 °C (Fig. 9C). This was also the case for $S_{C_2H_4}$ (35–38 %), S_{CH_4} (19.7–23.6 %) and $S_{C_2H_6}$ (1–1.8 %), whereas $S_{C_3H_6}$ (29–35 %) and S_{CO} (4.3–10 %) exhibited lower values compared to those obtained at 660 °C (Fig. 9D). Results imply that prolonged catalyst exposure to the gas stream and/or increase of reaction temperature led to a slight inhibition of the CO_2-ODP reaction favoring the undesired reactions of propane or propylene decomposition (8−11) and propane hydrogenolysis (12, 13).

The TOS stability for the CO_2-assisted oxidative dehydrogenation of propane was also investigated over Ga_2O_3-TiO_2 catalyst and results obtained are presented in Fig. 10. As it can be seen, $X_{C_3H_8}$ and $Y_{C_3H_6}$ measured at 660 °C remained constant with time on stream taking values of 22–26 % and 9–11 %, respectively (Fig. 10A). This was also the case for all products selectivities ($S_{C_3H_6}$=40–41 %, $S_{C_2H_4}$=34–36 %, S_{CH_4}=17–19 %, $S_{C_2H_6}$=0.7–0.8 %) with the exception of S_{CO} which was decreasing from ~7.9–4 % by the end of the day where the flow was switched and remained in He overnight. However, the initial values of S_{CO} were regained upon subsequent catalyst exposure to the reaction mixture (Fig. 10B).

A similar stability test was conducted at 710 °C and, as it was discussed in our previous study, Ga_2O_3-TiO_2 catalyst exhibited excellent stability for 25 hours on stream with $X_{C_3H_8}$ varied in the range of

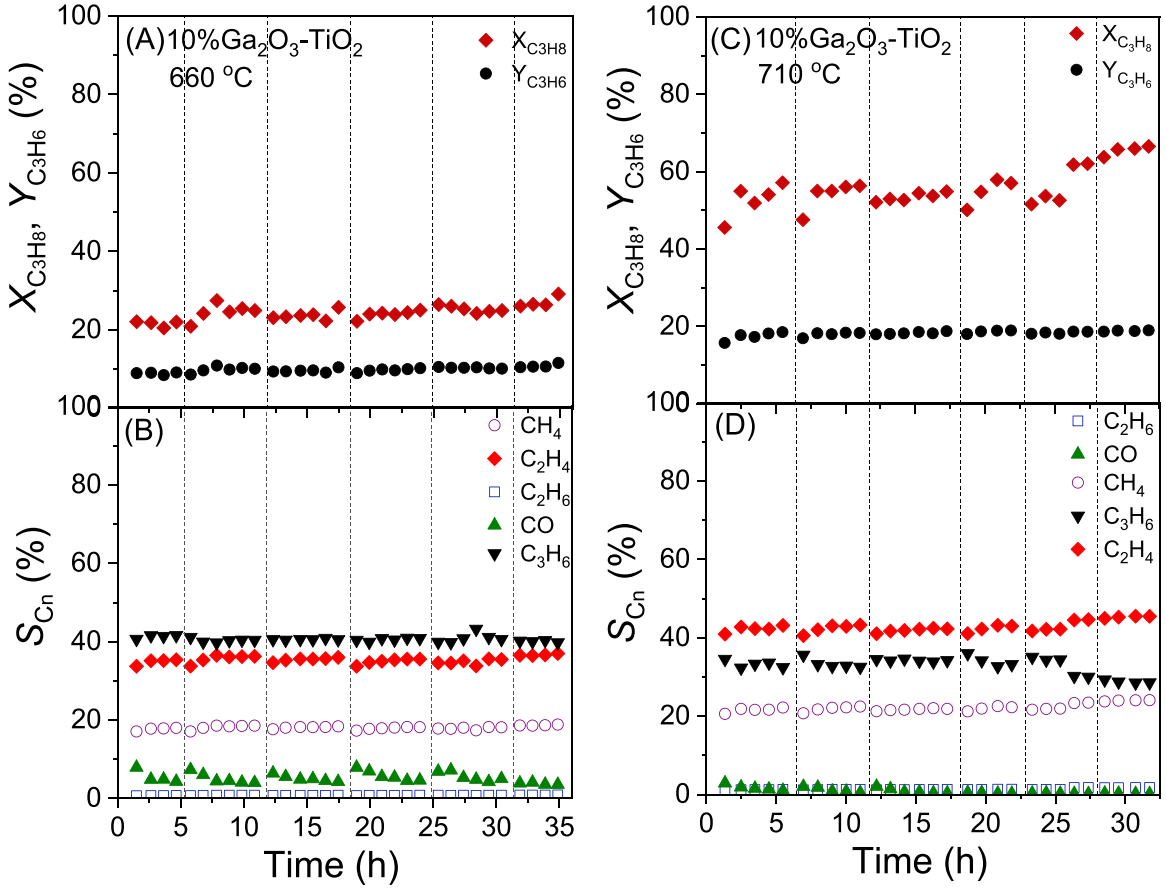

Fig. 10. TOS stability test of the 10 %Ga_2O_3-TiO_2 catalyst conducted at (A, B) 660 °C and (C, D) 710 °C under conditions of oxidative dehydrogenation of C_3H_8 with CO_2. Alterations of (A, C) $X_{C_3H_8}$ and $Y_{C_3H_6}$, and (B, D) products selectivity with time-on-stream. Experimental conditions: Same as in Fig. 5. Dashed vertical black lines indicate shutting down of the system overnight where the catalyst remained under He flow. (A) and (B) are reproduced from Ref [1].

52–57 % (Fig. 10C) [1]. However, increase of reaction time to 32 hours led to a gradual increase of propane conversion to 66.5 %. The observed increase of $X_{C_3H_8}$ influenced the variation of products selectivities with time, which although were found to be stable during the first 25 hours on stream ($S_{C_3H_6}$=32.5–36 %, S_{CO} =0.5–2 %, $S_{C_2H_4}$=40–43 % S_{CH_4}=20–22.5 %, $S_{C_2H_6}$~1 %) a slight increase of $S_{C_2H_4}$ (45.5 %) and S_{CH_4} (24 %) was observed with further increase of reaction time which was accompanied by a simultaneous $S_{C_3H_6}$ reduction to 28.5 % (Fig. 10D). Results indicate that the side reactions (9−14) promoting further production of C_2H_4 and CH_4 were facilitated after extended Ga_2O_3-TiO_2 interaction with the 5 %C_3H_8+25 %CO_2/He mixture. It should be noted however, that $Y_{C_3H_6}$ remained unaffected by the observed increase of propane conversion, taking values of 17–19 % during the whole stability test duration (Fig. 10C). As it was also observed for Ga_2O_3-SiO_2 catalyst (Fig. 9), higher reaction temperature hindered C_3H_6 formation and enhanced the production of the undesired C_2H_4 and CH_4 over Ga_2O_3-TiO_2 catalyst (Fig. 10).

Contrary to what observed over Ga_2O_3-SiO_2 and Ga_2O_3-TiO_2 catalysts, the interaction of Ga_2O_3-Al_2O_3 with the gas stream at 600 °C resulted in a progressive catalyst deactivation with the $X_{C_3H_8}$ and $Y_{C_3H_6}$ decreasing from 29 % to 7.3 % and from 21 % to 3.3 % after 18 hours on stream (Fig. 11A). It should be noted that the selection of a lower reaction temperature (600 °C) for the stability test conduction compared to that used (660 °C) for Ga_2O_3-SiO_2 and Ga_2O_3-TiO_2 catalysts was made in order to achieve comparable propane conversions since Ga_2O_3-Al_2O_3 exhibited significantly higher activity (Fig. 6). The gradual loss of catalytic activity was accompanied by a decrease of $S_{C_3H_6}$ from 72 % to 45 % and an increase of S_{CH_4} and $S_{C_2H_4}$ from 5 % to 10.5 %, and from 4.4 % to 20 %, respectively (Fig. 11B). This provides evidence that catalyst deactivation was possibly induced by carbon deposition taking place via propylene and propane decomposition (11, 12) reactions, which both favor methane and ethylene generation. The observed increase of S_{CO} (17.9–31.6 %) with time on stream was maybe due to the reverse Boudouard reaction (15) which converted part of the coke formed to CO (Fig. 11B). Selectivity towards ethane also exhibited an increase (from 0.18 % to 0.37 %) most possibly due to the parallel occurrence of propane hydrogenolysis (13). Interestingly, Ga_2O_3-Al_2O_3 catalyst exhibited excellent stability at 710 °C for 30 hours on stream with $X_{C_3H_8}$ and $Y_{C_3H_6}$ stabilizing at 57–60 % and 18–19 %, respectively, during the first 5 hours of reaction (Fig. 11C). Propylene selectivity was found to be constant (32–33 %) whereas those of ethylene, methane and ethane were progressively increased from 28 % to 45 %, from 18 % to 22 %, and from 0.9 % to 1.3 %, respectively, with time on stream. On the other hand, S_{CO} was significantly decreased from 30.7 % to 0.4 % after ~30 hours on stream. This may indicate that propylene was mainly produced via propane dehydrogenation rather than CO_2-assisted oxidative dehydrogenation as evidenced by the observed stable X_{C3H6} and $Y_{C_3H_6}$ in combination with an observed progressive decrease of X_{CO2} (not shown here) from 10 % to 1 %.

This implies that CO_2 participation in propane conversion was suppressed with time on stream when the reaction was taking place at 710 °C over Ga_2O_3-Al_2O_3 catalyst. This may be due to competitive adsorption of CO_2 on the same basic sites with one or more reaction products. According to the results reported by Davydov et al. [53], strong basic sites participate in methane activation for the reaction of oxidative coupling of methane. Similarly, the increased surface basicity was found to be responsible for the improved and selective conversion of methane towards C_{2+} hydrocarbons [77]. Thus, it can be suggested that

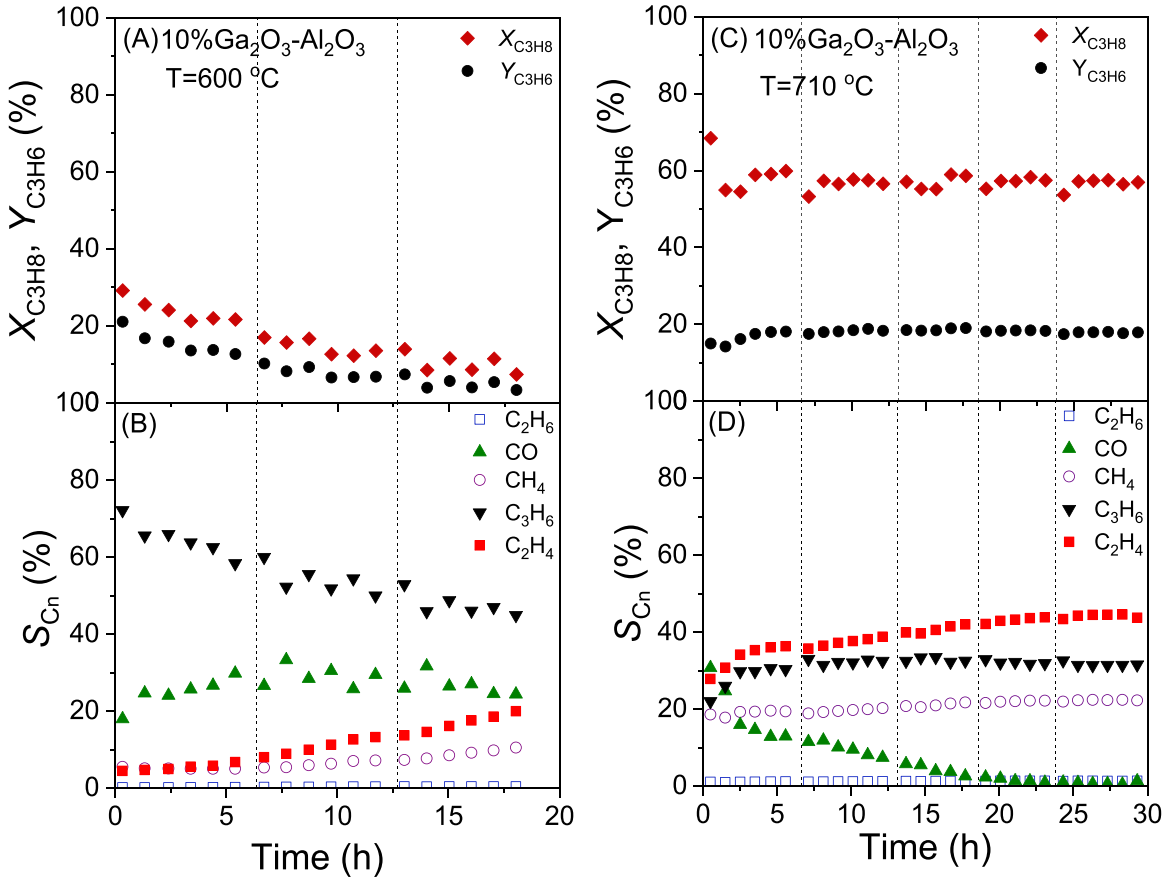

Fig. 11. TOS stability test of the 10 %Ga_2O_3-Al_2O_3 catalyst conducted at (A, B) 600 °C and (C, D) 710 °C under conditions of oxidative dehydrogenation of C_3H_8 with CO_2. Alterations of (A, C) $X_{C_3H_8}$ and $Y_{C_3H_6}$, and (B, D) products selectivity with time-on-stream. Experimental conditions: Same as in Fig. 5. Dashed vertical black lines indicate shutting down of the system overnight where the catalyst remained under He flow.

part of the produced CH_4 was accumulated on the catalyst surface hindering the activation of CO_2 and its participation in propane conversion to propylene.

Therefore, if the DP reaction dominates the CO_2-ODP at 710 °C, H_2O generation through reaction (3) was expected to be suppressed. This may explain the contradictory stable performance of Ga_2O_3-Al_2O_3 catalyst at 710 °C compared to its rapid deactivation at 600 °C, since the presence of water molecules has been suggested to be among the reasons of catalyst deactivation under CO_2-ODP conditions [3].

It should be noted that, with the exception of Ga_2O_3-Al_2O_3 catalyst which was found to be gradually deactivated with time when the reaction was taking place at 600 °C, the investigated catalysts exhibited sufficient stability for about 30–35 hours on stream contrary to previous studies where a rapid catalyst deactivation was observed. For example Xu et al. [8] found that the initial propane conversion measured for Ga_2O_3-Al_2O_3, Ga_2O_3-TiO_2 and Ga_2O_3-SiO_2 catalysts was significantly decreased with time on stream due to coke formation with all catalysts being practically inactive after 160 min. A drastic catalyst deactivation during the first 45 minutes on stream at 600 °C was also observed by Gashoul Daresibi et al. [14] over Ga_2O_3-Al_2O_3 catalyst prepared employing the atomic layer deposition method. This deactivation was attributed either to the higher number of acidic sites which promotes coke formation or to migration of incorporated Ga to the surface under reaction conditions, leading to surface reconstruction through the formation of Ga_2O_3 particles characterized by lower activity and weak interaction with the alumina support. A rapid decrease of propane conversion from 50 to ~21 % after 16 hours of reaction was also reported by Chen et al. [16] over Ga_2O_3-Al_2O_3 catalyst with Ga/Al ratio of 4:1 at 500 °C. The rate of catalyst deactivation was increased with increasing the reaction temperature and time and was assigned to acceleration of carbon deposition. Although the deactivation effects were eliminated for Ga/Al ratios of 1:4 and 1:1, propane conversion and propylene yield were found to be lower. Similarly, Xiao et al. [15] found that Ga_2O_3-Al_2O_3 catalysts synthesized by three different methods (hydrothermal, grind-mixture and coprecipitation) were deactivated after 9 hours on stream at 550 °C due to coke deposition.

3.4. X-ray diffraction measurements obtained over "spent" catalysts

In an attempt to clarify the effect of support on variations of products selectivity and/or catalyst deactivation with time on stream all "spent" catalysts following the stability tests were characterized by XRD technique and results obtained are presented in Fig.S7. It was observed that, in all cases, the XRD patterns obtained from the "spent" catalysts are qualitatively similar with those obtained from the corresponding "fresh" samples with respect of the detected crystallographic peaks. The primary crystallite size of Ga_2O_3-Al_2O_3 was not altered after the stability tests conducted at 600 and 710 °C, taking values of 6.9 and 6.3 nm, respectively. Contrary, prolonged interaction of Ga_2O_3-TiO_2 catalyst with the reaction mixture at 660 and 710 °C led to an increase of the TiO_2 crystallite size from 18.3 nm to 21.4 and 22.3 nm, respectively, for the anatase phase, and from 14.9 nm to 28.7 and 32.3 nm, respectively, for the rutile phase. The anatase content remained stable (78–79 %) after 30 hours on stream at both reaction temperatures investigated. Results imply that titania particles were sintered under reaction conditions without, however, affecting significantly the catalytic performance which remained almost constant with time on stream. In our previous study it was demonstrated that propylene production via ODP with CO_2 reaction was favored over small TiO_2 crystallites [1]. Therefore, it can be suggested that the increase of titania particles size may be related, at least in part, to the observed small decrease of $S_{C_3H_6}$ after 25 hours on stream at 710 °C. It is of interest to note that no crystallographic peaks assigned to carbon was detected for any of the "spent" catalysts examined indicating that either the amount of coke was small and/or the deposited coke was in an amorphous phase [78].

3.5. Transmission electron microscopy measurements

The morphology of the "fresh" and "spent" supported gallium oxide catalysts was studied by Transmission Electron Microscopy. TEM images obtained from Ga_2O_3-SiO_2 catalysts are presented in Fig.S8 where it is observed that the "fresh" sample (Fig.S8A) was characterized by irregular spherical particles. Prolonged catalyst exposure to the reaction mixture at 660 and 710 °C did not induce any significant variation in its structural characteristics (Fig.S8B and C). Selected area electron diffraction (SAED) pattern recorded from the area shown with dashed lines in the corresponding TEM image is presented only for the "spent" sample after the TOS stability test at 710 °C (Ga_2O_3-SiO_2_Spent 710 °C, Fig.S8D) due to inability to receive diffraction rings in the case of the "fresh" (Ga_2O_3-SiO_2_Fresh) and the "spent" sample after the TOS stability test at 660 °C (Ga_2O_3-SiO_2_Spent 660 °C). The ring denoted by spot 1 (Fig. S8D) corresponds to (201) plane of tetragonal SiO_2 (JCPDS Card No. 32–993) in agreement with the XRD results (Fig. 1).

A representative TEM image obtained from the "fresh" Ga_2O_3-TiO_2 catalyst (Ga_2O_3-TiO_2_Fresh) is shown in Fig.S9A where irregular spherical TiO_2 particles of approximately 18–20 nm diameter can be observed. Regarding the corresponding SAED analysis (Fig.S9B), the observed diffraction rings mentioned by spot 1, 2, 3, 4, 5, 6 and 7 correspond to d-spacing 3.51, 2.43, 2.33, 1.89, 1.7, 1.49 and 1.36 Å attributed to (101), (103), (112), (200), (105), (213) and (116) Miller indices of anatase phase (JCPDS Card No. 4–477), respectively. Catalyst interaction with the reaction mixture at 660 and 710 °C for ~35 hours resulted in the development of larger titania nanoparticles with a mean size of 23 nm and 24 nm, respectively as evidenced by the TEM images presented in Figs.S9C and E in excellent agreement with XRD results (Fig.S7). Regarding the analysis of the electron diffractogram of the "spent" sample following the TOS stability experiment at 660 °C (Ga_2O_3-TiO_2_Spent 660 °C, Fig. S9D), the spots 1, 2, 3, 4, 5, 6, 7, 8 and 9 correspond to (101), (103), (112), (200), (105), (213), (116), (215) and (303) facets of anatase titania (JCPDS Card No. 4–477), respectively, whereas the spots 1, 2, 3, 4, 5 and 6 recorded for the Ga_2O_3-TiO_2 sample following the TOS stability experiment at 710 °C (Ga_2O_3-TiO_2_Spent 710 °C, Fig. S9F) are due to (101), (112), (105), (213), (116) and (215) planes of anatase titania (JCPDS Card No. 4–477), respectively. Crystallographic rings attributed to the rutile phase of TiO_2 were not detected via SAED analysis for both the "fresh" (Fig. S9B) and "spent" (Figs. S9D and F) samples, contrary to XRD measurements where the characteristic crystallographic peaks assigned to the rutile phase were identified. This may be due to the smaller rutile content (~21–22 %) compared to that of anatase (78–79 %) for both "fresh" and "spent" titania-supported catalysts.

The TEM images and the selected area electron diffractograms obtained for the "fresh" (Ga_2O_3-Al_2O_3_Fresh) and "spent" Ga_2O_3-Al_2O_3 (Ga_2O_3-Al_2O_3_Spent 600 °C, Ga_2O_3-Al_2O_3_Spent 710 °C) samples showed that all catalysts are composed of Al_2O_3 spherical nanoparticles with an approximate diameter of 6–8 nm (Fig. 12). Concerning the SAED spectrum of the "fresh" sample (Fig. 12B) each spot corresponds to a specific facet of the Al_2O_3 structure (JCPDS Card No. 2–1422). Specifically, spots 1, 2, 3, 4, 5 and 6 are attributed to reflections of the planes with a d-spacing value equal to 3, 2.4, 1.98, 1.63, 1.43 and 1.39 Å of an unknown Al_2O_3 structure. This was also the case for both the Ga_2O_3-Al_2O_3_Spent 600 °C (Fig. 12D) and Ga_2O_3-Al_2O_3_Spent 710 °C (Fig. 12F) samples. Contrary to SAED analysis, XRD results demonstrated a cubic Al_2O_3 structure for both the "fresh" and "spent" Ga_2O_3-Al_2O_3 catalysts. These findings may imply that the structure of alumina used as support was polycrystalline.

It should be noted that for all gallium oxide-support combinations employed no reflections attributed to Ga_2O_3 structure or carbon formations (for the "spent" samples) were detected, corroborating the XRD measurements and further supporting our previous suggestion that gallium oxide particles are well dispersed [10] and that the carbon deposited on the catalytic surface during reaction was amorphous [79].

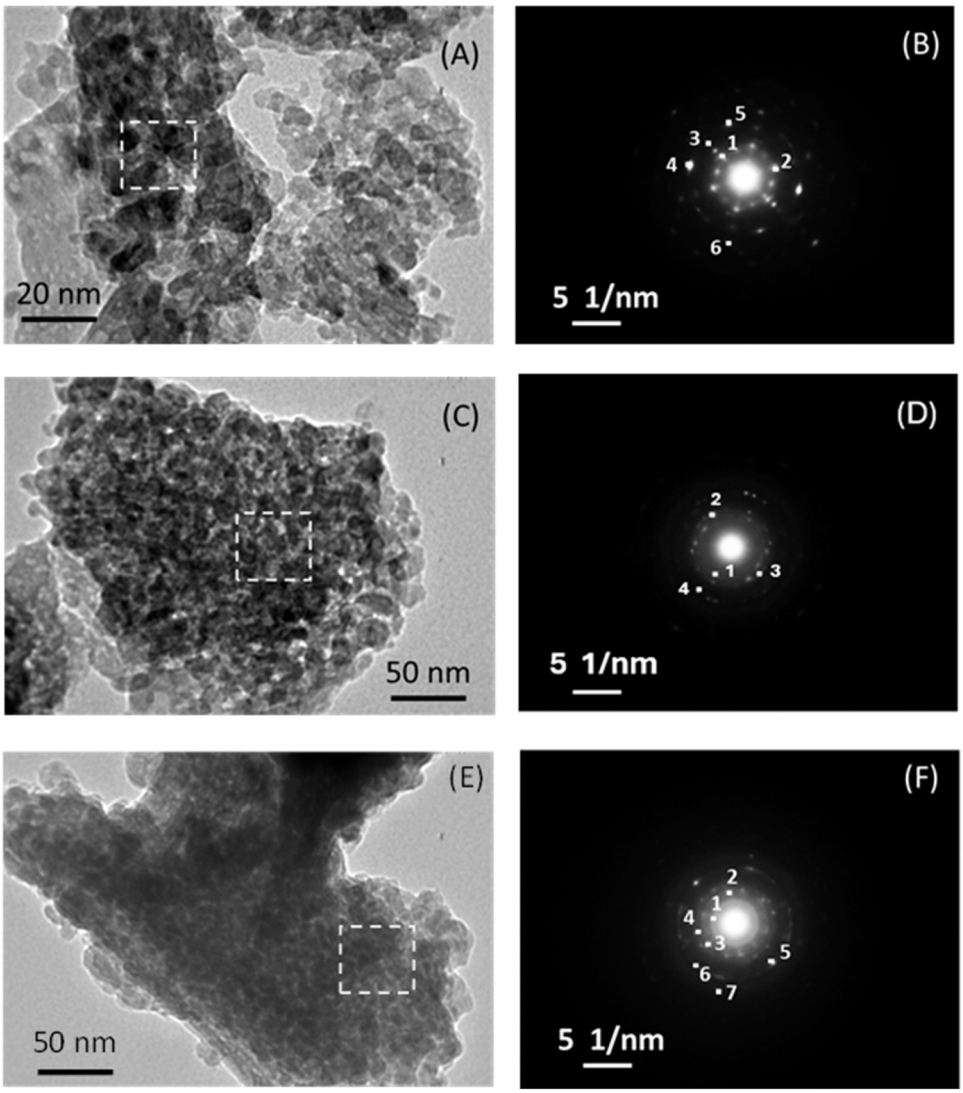

Fig. 12. TEM micrographs of the (A) "fresh" and (C and E) "spent" 10 % Ga_2O_3-Al_2O_3 catalysts following TOS test at 600 °C and 710 °C. Corresponding selected area electron diffractograms for the (B) "fresh" and (D and F) "spent" samples at 600 °C and 710 °C acquired from the area denoted by the dashed lines in (A), (C) and (E), respectively.

3.6. Scanning electron microscopy measurements

The morphology and the distribution of the elements contained in the synthesized catalysts were examined with SEM, and representative images obtained from the "fresh" Ga_2O_3-SiO_2, Ga_2O_3-TiO_2 and Ga_2O_3-Al_2O_3 catalysts are shown in Fig. 13A, B and C. The corresponding energy-dispersive X-ray spectra (EDS) of these SEM images (Fig. 13G, H and I) confirmed the presence of Ga, O and Si or Ti or Al elements, whereas elements quantification demonstrated that the Ga content (wt %) was practically the same (5–6 wt%) for the three catalysts examined (Table S3). Elemental mapping illustrates that Ga was homogeneously distributed on the surface of Al_2O_3, TiO_2 or SiO_2 (Fig. 13D, E and F).

Similar SEM/EDS analysis was conducted over all "spent" catalysts investigated. Results obtained from "spent" Ga_2O_3-SiO_2 catalysts are presented in Fig.S10. The element mapping for Si (Fig.S10C and F), Ga (Fig.S10D and G) and C (Fig.S10E and H) indicated that the Si and Ga are uniformly present on both "spent" samples whereas carbon was uniformly deposited on their surface. The weight percentage of Si, Ga, O and C estimated by the EDS analysis (Fig. S10I and J) for the Ga_2O_3-SiO_2_Spent 660 °C catalyst was found to be equal to ca. 40 wt%, 7 wt%, 43 wt% and 10 wt%, respectively, while that for the Ga_2O_3-SiO_2_Spent 710 °C was equal to 14 wt%, 2 wt%, 29 wt% and 55 wt%, respectively (Table S3). Results clearly show that the amount of carbon formed on the catalyst surface after prolonged catalyst exposure to the gas stream was significantly higher when the reaction was taking place at 710 °C compared to 660 °C, implying that the undesired reactions leading to coke formation were facilitated at higher reaction temperatures in agreement with results of Figs. 7 and 9.

SEM/EDS results obtained from the "spent" Ga_2O_3-TiO_2 catalysts are presented in Fig.S11 where it can be observed that the uniform presence of Ti and Ga was retained following the TOS stability tests at 660 °C (Fig. S11C and D) and 710 °C (Fig.S11F and G). The coke formed under reaction conditions was homogeneously distributed on the catalysts' surface (Fig.S11E and H) and found to be significantly higher (26 wt%) for the Ga_2O_3-TiO_2_Spent 710 °C than that measured (8 wt%) for the Ga_2O_3-TiO_2_Spent 660 °C sample in accordance to the results discussed above for Ga_2O_3-SiO_2 (Table S3). Qualitatively similar results were obtained over the "spent" Ga_2O_3-Al_2O_3 catalysts with Ga and Al being uniformly present and the deposited carbon being homogeneously distributed on the surface of both samples and higher over the Ga_2O_3-Al_2O_3_Spent 710 °C (15 wt%) compared to Ga_2O_3- Al_2O_3_Spent 600 °C (9 wt%) (Fig. 14, Table S3).

It should be noted that in all cases the variations observed in the content of Ga and Si or Ti or Al between the "fresh" and the "spent"

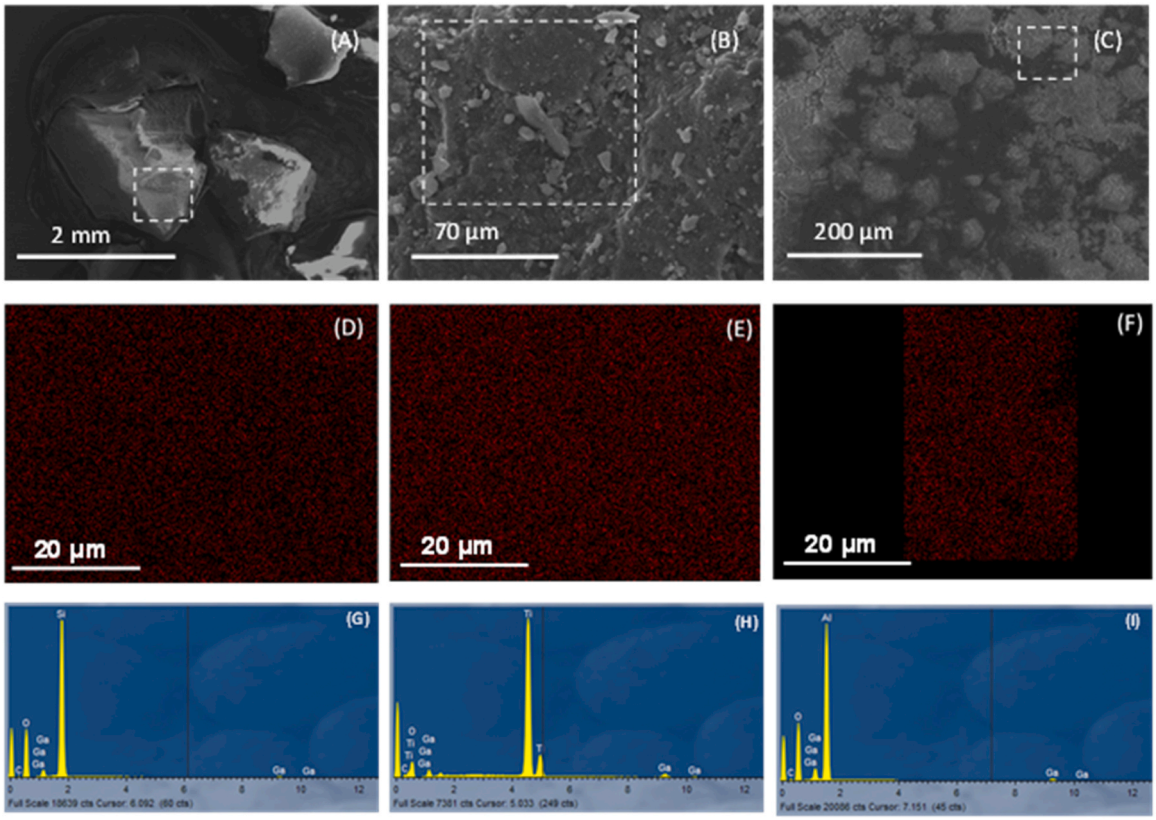

Fig. 13. SEM images with element mapping of Ga and EDS profiles obtained from the "fresh" (A, D, G) 10 % Ga_2O_3-SiO_2 (B, E, H) 10 % Ga_2O_3-TiO_2 and (C, F, I) 10 % Ga_2O_3-Al_2O_3 catalysts.

samples could be attributed to the carbon deposition becoming more pronounced as the reaction temperature increased (Table S3).

3.7. Temperature programmed oxidation measurements

Comparison between results of TOS stability experiments and SEM analysis shows that Ga_2O_3-Al_2O_3 catalyst lost rapidly its initial activity, when the reaction occurred at 600 °C, despite the comparable values of carbon content (8–10 wt%) found based on EDS analysis of the three catalysts investigated. In order to accurately estimate the amount of carbon deposited on the catalyst surface under reaction conditions, TPO experiments were performed over the Ga_2O_3-Al_2O_3_Spent 600 °C, Ga_2O_3-TiO_2_Spent 660 °C and Ga_2O_3-SiO_2_Spent 660 °C catalysts and results obtained are illustrated in Fig. 15A. The profile of CO_2 produced during a linear increase of temperature (10 °C/min) under a 3 % O_2/He stream exhibited, for all catalysts, a single peak with its maximum being varied with respect to the support nature following the order Al_2O_3 (T_{max}=549 °C) < TiO_2 (T_{max}=574 °C) < SiO_2 (T_{max}=685 °C). Similar peaks were previously attributed to oxidation of amorphous carbonaceous deposits [80,81]. In all cases the production of CO was negligible.

The opposite trend with that of T_{max} was observed concerning the amounts (µmol g^{-1}) of CO_2 produced during TPO experiments (estimated by the area below the CO_2 response curve) which was estimated to be 4000 µmol g^{-1} for Ga_2O_3-SiO_2, 6000 µmol g^{-1} for Ga_2O_3-TiO_2 and 7000 µmol g^{-1} for Ga_2O_3-Al_2O_3. Results indicate that carbon deposition was significantly enhanced over Ga_2O_3-Al_2O_3 which may be responsible for the deactivation observed in Fig. 11A and B. This may be due to the higher surface acidity of this catalyst, which according to previous studies promotes coke formation, leading to gradually loss of activity with time on stream [14,15,60,82]. It should be mentioned that, the evolution of CO_2 at higher temperatures over Ga_2O_3-TiO_2 and, especially, Ga_2O_3-SiO_2 provides evidence that carbon formation on the surface of these catalysts was more stable compared to Ga_2O_3-Al_2O_3, leading to lower carbon oxidation rate during the TPO experiment. This may imply that besides the higher amount of coke formation when Al_2O_3 was used as support, the gasification of carbon (e.g. via the reverse Boudouard reaction) may be facilitated over this sample under reaction conditions in accordance to the observed increase of S_{CO} (Fig. 11B) with time on stream, which however, was not sufficient to avoid catalyst deactivation.

It should be noted that Ga_2O_3-Al_2O_3 deactivation due to reconstruction of the catalytic surface under reaction conditions proposed by Gashoul Daresibi et al. [14] and/or by water molecules generated during CO_2-ODP reaction [3] cannot not be excluded although cannot be confirmed based on the results of the present study. As discussed above, the latter approach could explain the stable performance of Ga_2O_3-Al_2O_3 catalyst at 710 °C where propylene was mainly produced via DP reaction rather than CO_2-ODP reaction (Fig. 11C and D), suppressing water generation through reaction (3). Furthermore, propane aromatization which is promoted by the presence of both strong acid sites and Ga species may be responsible for the short life time of Ga_2O_3-Al_2O_3 catalyst [60,82,83]. In any case, results of the present study clearly show that an appropriate balance between the acid and basic sites is essential in order propane conversion to propylene to be enhanced and simultaneously catalyst stability to be ensured hindering any deactivation phenomena.

Similar TPO experiments were conducted for the samples obtained following the TOS stability tests at 710 °C. Results showed that, in all cases, CO_2 production initiated above 550 °C after exposure of spent catalysts to 3 %O_2/He stream indicating that carbon was strongly adsorbed on the catalyst surface (Fig. 15B). All catalysts had to remain at 800 °C for a long time (20–50 min) until the whole amount of carbon to be oxidized to CO_2. Comparison with the results presented in Fig. 15A showed that the amount of carbon deposited on the catalyst surface was higher when the stability test was conducted at 710 °C, which was rather

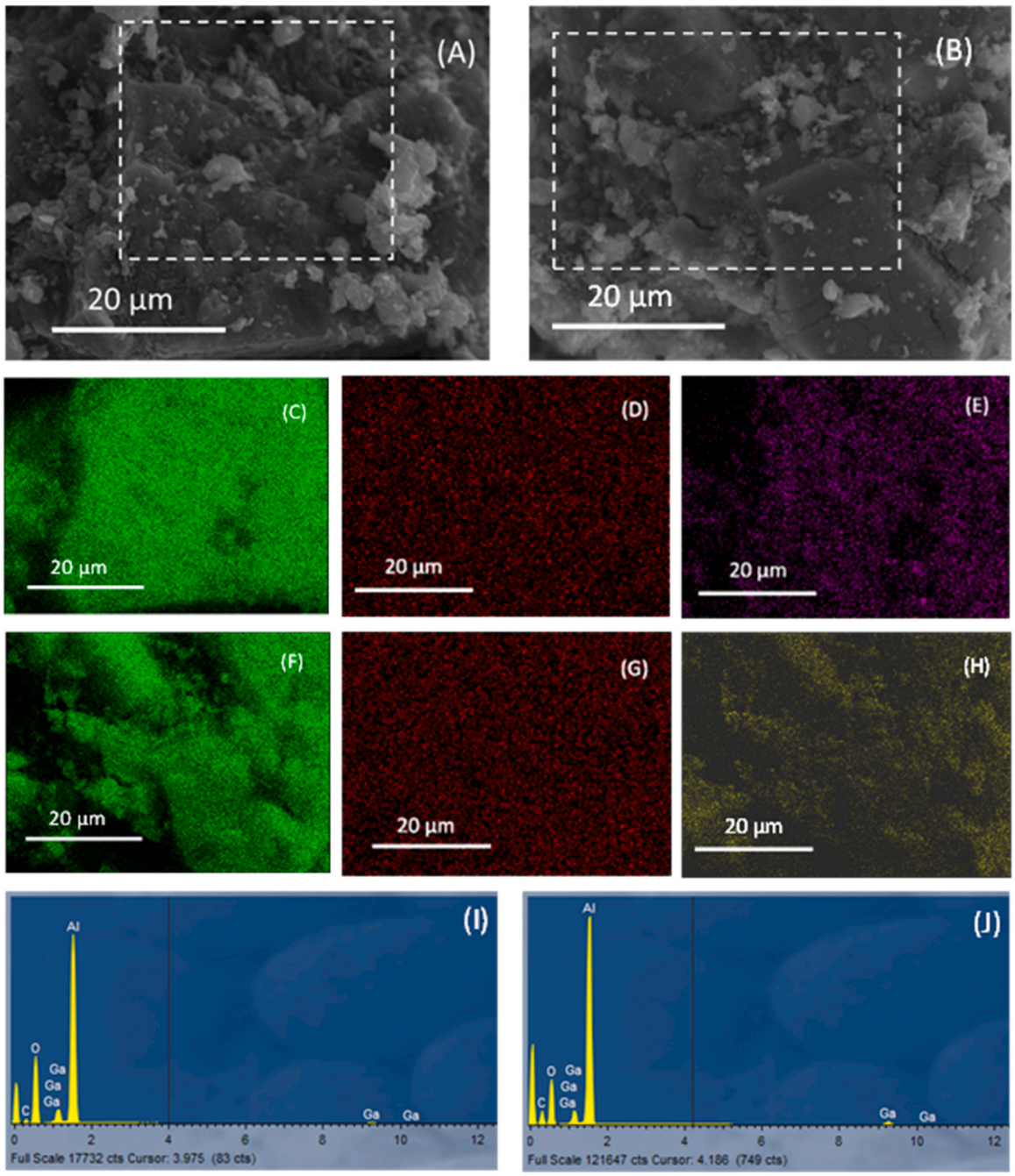

Fig. 14. SEM images of the "spent" 10 % Ga_2O_3-Al_2O_3 catalyst obtained following the TOS stability tests at (A) 600 °C and (B) 710 °C. EDS mapping results showing the distribution of (C) Al, (D) Ga and (E) carbon elements and (I) the corresponding EDS spectrum for the "spent" sample tested at 600 °C. EDS mapping results showing the distribution of (F) Al, (G) Ga and (H) carbon elements and (J) the corresponding EDS spectrum for the "spent" sample tested at 710 °C.

expected since the selectivity towards side products accompanied by carbon formation was enhanced with increasing temperature (Fig. 7). Silica supported catalyst exhibited the highest tendency to coke formation (18476 μmol g^{-1}), in agreement with EDS analysis (Table S3), followed by Ga_2O_3-Al_2O_3 (16812 μmol g^{-1}) and subsequently Ga_2O_3-TiO_2 (11084 μmol g^{-1}). Results indicated that the catalyst ranking with respect to their resistance to carbon deposition was different at 710 °C compared to 600 (or 660) °C. In any case, carbon formation at 710 °C was not able to deactivate any of the investigated catalysts even after 30–35 hours on stream which is of significant importance for the practical application of the CO_2-ODP process.

In an attempt to determine the selectivity of catalysts towards carbon deposition, we estimated the ratio of the amount of carbon formed at the end of each TOS stability test to the mean C_3H_8 converted per unit time, $S_{C/X_{C_3H_8}}$ (in μmol g^{-1} h^{-1}). It was found that the $S_{C/X_{C_3H_8}}$ depended on the reaction temperature and increased in the order (a) SiO_2 (516.1 μmol g^{-1} h^{-1}) < TiO_2 (586.1 μmol g^{-1} h^{-1}) < Al_2O_3 (2397.6 μmol g^{-1} h^{-1}) for the low temperature TOS stability test and (b) TiO_2 (626.1 μmol g^{-1} h^{-1}) < SiO_2 (807.5 μmol g^{-1} h^{-1}) < Al_2O_3 (1001.7 μmol g^{-1} h^{-1}) for the high temperature TOS test, indicating that the alumina supported catalyst exhibited the lowest anti-coke ability under CO_2-ODP conditions.

4. Conclusions

The production of propylene via the CO_2-ODP reaction over gallium oxide dispersed on SiO_2, TiO_2 and Al_2O_3 supports was reported herein

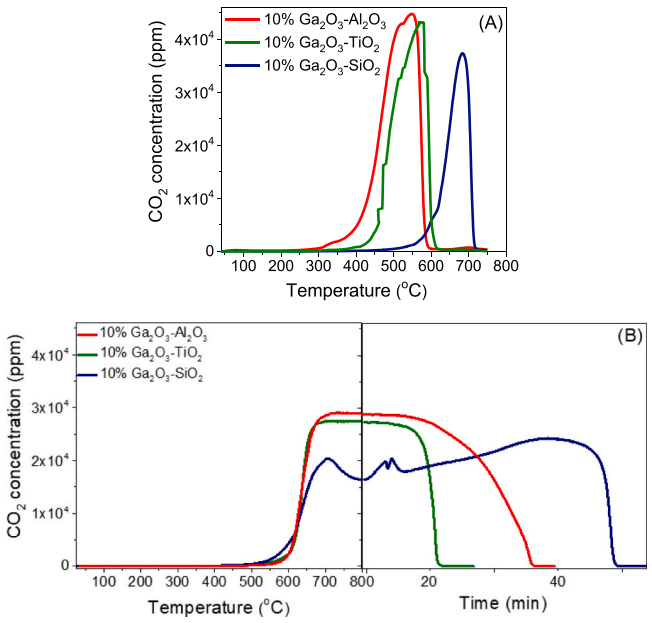

Fig. 15. Responses of CO_2 produced during temperature programmed oxidation with 3 %O_2 (in He) occurred after the TOS stability tests presented in Figs. 8–10 conducted at (A) 600 °C over 10 % Ga_2O_3-Al_2O_3 catalyst and 660 °C over 10 % Ga_2O_3-SiO_2 and 10 % Ga_2O_3-TiO_2 catalysts and (B) 710 °C over 10 % Ga_2O_3-Al_2O_3, 10 % Ga_2O_3-SiO_2 and 10 % Ga_2O_3-TiO_2 catalysts. In (B), CO_2 responses above 800 °C were recorded as a function of time since catalysts needed to remain at 800 °C for 20–50 min until complete oxidation of carbon.

attempting to identify the effect of the support on both catalytic activity and stability. SEM/EDS analysis performed over the "fresh" samples illustrated that Ga was homogeneously distributed on the surface of Al_2O_3, TiO_2 or SiO_2 support. No reflections attributed to Ga_2O_3 structure was detected by TEM/SAED and XRD measurements indicating that gallium oxide particles were well dispersed. Both propane conversion and propylene yield were found to be higher when gallium oxide was dispersed on alumina support which was characterized by the highest acid site density and moderate number of basic sites. Low reaction temperatures favored the conversion of C_3H_8 towards C_3H_6 which was hindered above 650 °C where the undesired reactions of C_3H_8 or C_3H_6 decomposition and C_3H_8 hydrogenolysis were facilitated yielding C_2H_4 and CH_4 and promoting coke formation on the catalyst surface. The TOS stability tests demonstrated that all catalysts exhibited sufficient stability for ~30–35 hours with the exception of Ga_2O_3-Al_2O_3 at 600 °C which became practically inactive after 18 hours on stream due to enhanced coke formation, as measured by TPO experiments, induced by the increased surface acidity of this catalyst. EDS analysis also confirmed the formation of carbon which was found to increase with increasing temperature in agreement with TPO results. The tendency of catalysts towards carbon deposition with respect to the support nature was altered when the TOS stability test was conducted at 710 °C, which however was not able to deactivate any of the investigated samples. No carbon formation was detected by conducting TEM and XRD experiments over all the "spent" catalysts investigated providing evidences that the so formed carbon was amorphous. Results of the present study demonstrated that the role of the support in the CO_2-ODP process is to provide the appropriate number of active acid/base sites, which can be significantly modified via its interaction with gallium oxide particles, thus affecting catalytic activity, selectivity and stability.

CRediT authorship contribution statement

Alexandra Florou: Investigation, Data curation. **Georgios Bampos:** Investigation, Data curation. **Panagiota D. Natsi:** Investigation. **Aliki Kokka:** Investigation, Data curation. **Paraskevi Panagiotopoulou:** Writing – review & editing, Writing – original draft, Visualization, Validation, Supervision, Project administration, Methodology, Investigation, Funding acquisition, Formal analysis, Data curation, Conceptualization.

Declaration of Competing Interest

The authors declare that they have no known competing financial interests or personal relationships that could have appeared to influence the work reported in this paper.

Acknowledgements

The research project was supported by the Hellenic Foundation for Research and Innovation (H.F.R.I.) under the "2nd Call for H.F.R.I. Research Projects to support Faculty Members & Researchers" (Project Number: 3367). The authors would like to thank M. Kollia and K. Govatsi, staff of the Laboratory of Electron Microscopy and Microanalysis (L.E.M.M.) at the University of Patras for TEM and SEM images.

Appendix A. Supporting information

Supplementary data associated with this article can be found in the online version at doi:10.1016/j.jece.2024.114603.

Data availability

The data that has been used is confidential.

References

[1] A. Florou, G. Bampos, P.D. Natsi, A. Kokka, P. Panagiotopoulou, Propylene production via oxidative dehydrogenation of propane with carbon dioxide over composite M_xO_y-TiO_2 catalysts, Nanomaterials 14 (2024) 86, https://doi.org/10.3390/nano14010086.
[2] K. Zhang, S. Sun, K. Huang, Combined carbon capture and catalytic oxidative dehydrogenation of propane to propylene conversion through a plug-flow dual-phase membrane reactor, Chem. Eng. J. 481 (2024) 148395, https://doi.org/10.1016/j.cej.2023.148395.
[3] H. Wang, X. Zhang, Z. Su, T. Chen, Dealuminated Beta stabilized bimetallic PtCo nanoparticles for oxidative dehydrogenation of propane with CO_2, Fuel 358 (2024) 130248, https://doi.org/10.1016/j.fuel.2023.130248.
[4] S. Chen, X. Chang, G. Sun, T. Zhang, Y. Xu, Y. Wang, C. Pei, J. Gong, Propane dehydrogenation: catalyst development, new chemistry, and emerging technologies, Chem. Soc. Rev. 50 (2021) 3315–3354, https://doi.org/10.1039/D0CS00814A.
[5] I. Chung, H. Jeong, D. Lee, J. Oh, O. Seo, A. Tayal, Y. Yun, Effect of Mo content on oxidative dehydrogenation of propane with CO_2 over ZnO_x catalysts supported on Mo–Zr mixed–oxides, Catal. Today 425 (2024) 114340, https://doi.org/10.1016/j.cattod.2023.114340.
[6] X. Zhang, J. Li, W. Liu, Y. Zheng, J. An, W. Xin, Z. Liu, L. Xu, X. Li, X. Zhu, Synergistic effect of zinc and iron in the CO_2-assisted oxidative dehydrogenation of propane, ACS Catal. 13 (2023) 14864–14873, https://doi.org/10.1021/acscatal.3c04371.
[7] M. Kocoń, P. Michorczyk, J. Ogonowski, Effect of supports on catalytic activity of chromium oxide-based catalysts in the dehydrogenation of propane with CO_2, Catal. Lett. 101 (2005) 53–57, https://doi.org/10.1007/s10562-004-3749-6.
[8] B. Xu, B. Zheng, W. Hua, Y. Yue, Z. Gao, Support effect in dehydrogenation of propane in the presence of CO_2 over supported gallium oxide catalysts, J. Catal. 239 (2006) 470–477, https://doi.org/10.1016/j.jcat.2006.02.017.
[9] I. Takahara, M. Saito, M. Inaba, K. Murata, Dehydrogenation of propane over a silica-supported vanadium oxide catalyst, Catal. Lett. 102 (2005) 201–205, https://doi.org/10.1007/s10562-005-5856-4.
[10] M.A. Tedeeva, A.L. Kustov, P.V. Pribytkov, G.I. Kapustin, A.V. Leonov, O. P. Tkachenko, O.B. Tursunov, N.D. Evdokimenko, L.M. Kustov, Dehydrogenation of propane in the presence of CO_2 on GaO_x/SiO_2 catalyst: influence of the texture characteristics of the support, Fuel 313 (2022) 122698, https://doi.org/10.1016/j.fuel.2021.122698.
[11] X. Zhang, Y. Yue, Z. Gao, Chromium oxide supported on mesoporous SBA-15 as propane dehydrogenation and oxidative dehydrogenation catalysts, Catal. Lett. 83 (2002) 19–25, https://doi.org/10.1023/A:1020693028720.
[12] Y. Gambo, S. Adamu, R.A. Lucky, M.S. Ba-Shammakh, M.M. Hossain, Decoupling reaction network and designing robust VO_x/Al_2O_3 catalyst with suitable site diversity for promoting CO_2-mediated oxidative dehydrogenation of propane, Chem. Eng. J. 479 (2024) 147458, https://doi.org/10.1016/j.cej.2023.147458.

[13] M. Chen, J. Xu, F.-Z. Su, Y.-M. Liu, Y. Cao, H.-Y. He, K.-N. Fan, Dehydrogenation of propane over spinel-type gallia–alumina solid solution catalysts, J. Catal. 256 (2008) 293–300, https://doi.org/10.1016/j.jcat.2008.03.021.

[14] F. Gashoul Daresibi, A.A. Khodadadi, Y. Mortazavi, Atomic layer deposition of Ga_2O_3 on γ-Al_2O_3 catalysts with higher interactions and improved activity and propylene selectivity in CO_2-assisted oxidative dehydrogenation of propane, Appl. Catal. A: Gen. 655 (2023) 119117, https://doi.org/10.1016/j.apcata.2023.119117.

[15] H. Xiao, J. Zhang, P. Wang, X. Wang, F. Pang, Z. Zhang, Y. Tan, Dehydrogenation of propane over a hydrothermal-synthesized Ga_2O_3–Al_2O_3 catalyst in the presence of carbon dioxide, Catal. Sci. Technol. 6 (2016) 5183–5195, https://doi.org/10.1039/C5CY02161H.

[16] M. Chen, J. Xu, Y.-M. Liu, Y. Cao, H.-Y. He, J.-H. Zhuang, K.-N. Fan, Enhanced activity of spinel-type Ga_2O_3–Al_2O_3 mixed oxide for the dehydrogenation of propane in the presence of CO_2, Catal. Lett. 124 (2008) 369–375, https://doi.org/10.1007/s10562-008-9478-5.

[17] H. Li, Y. Yue, C. Miao, Z. Xie, W. Hua, Z. Gao, Dehydrogenation of ethylbenzene and propane over Ga_2O_3–ZrO_2 catalysts in the presence of CO_2, Catal. Commun. 8 (2007) 1317–1322, https://doi.org/10.1016/j.catcom.2006.11.034.

[18] E.-H. Yuan, Y. Niu, X. Huang, M. Li, J. Bao, Y.-H. Song, B. Zhang, Z.-T. Liu, M.-G. Willinger, Z.-W. Liu, Finned Zn-MFI zeolite encapsulated noble metal nanoparticle catalysts for the oxidative dehydrogenation of propane with carbon dioxide, J. Energy Chem. 80 (2023) 479–491, https://doi.org/10.1016/j.jechem.2023.01.055.

[19] M. Igonina, M. Tedeeva, K. Kalmykov, G. Kapustin, V. Nissenbaum, I. Mishin, P. Pribytkov, S. Dunaev, L. Kustov, A. Kustov, Properties of CrO_x/MCM-41 and its catalytic activity in the reaction of propane dehydrogenation in the presence of CO_2, Catalysts 13 (2023) 906, https://doi.org/10.3390/catal13050906.

[20] W. Zhou, Y. Jiang, Z. Sun, S. Zhou, E. Xing, Y. Hai, G. Chen, Y. Zhao, Support effect of Ga-based catalysts in the CO_2-assisted oxidative dehydrogenation of propane, Catalysts 13 (2023) 896, https://doi.org/10.3390/catal13050896.

[21] Z.-Y. Wang, Z.-H. He, L.-Y. Li, S.-Y. Yang, M.-X. He, Y.-C. Sun, K. Wang, J.-G. Chen, Z.-T. Liu, Research progress of CO_2 oxidative dehydrogenation of propane to propylene over Cr-free metal catalysts, Rare Met. 41 (2022) 2129–2152, https://doi.org/10.1007/s12598-021-01959-y.

[22] M.A. Atanga, F. Rezaei, A. Jawad, M. Fitch, A.A. Rownaghi, Oxidative dehydrogenation of propane to propylene with carbon dioxide, Appl. Catal. B: Environ. 220 (2018) 429–445, https://doi.org/10.1016/j.apcatb.2017.08.052.

[23] A. Kokka, A. Petala, P. Panagiotopoulou, Support effects on the activity of ni catalysts for the propane steam reforming reaction, Nanomaterials 11 (2021) 1948, https://doi.org/10.3390/nano11081948.

[24] T. Ramantani, G. Bampos, A. Vavatsikos, G. Vatskalis, D.I. Kondarides, Propane steam reforming over catalysts derived from noble metal (Ru, Rh)-substituted $LaNiO_3$ and $La_{0.8}Sr_{0.2}NiO_3$ perovskite precursors, Nanomaterials 11 (2021) 1931, https://doi.org/10.3390/nano11081931.

[25] K.-i Shimizu, M. Takamatsu, K. Nishi, H. Yoshida, A. Satsuma, T. Tanaka, S. Yoshida, T. Hattori, Alumina-supported gallium oxide catalysts for NO selective reduction: influence of the local structure of surface gallium oxide species on the catalytic activity, J. Phys. Chem. B 103 (1999) 1542–1549, https://doi.org/10.1021/jp983790w.

[26] A. Jawad, S. Ahmed, Analysis and process evaluation of metal dopant (Zr, Cr)-promoted Ga-modified ZSM-5 for the oxidative dehydrogenation of propane in the presence and absence of CO_2, RSC Adv. 13 (2023) 11081–11095, https://doi.org/10.1039/D2RA08235G.

[27] R. Koirala, R. Buechel, F. Krumeich, S.E. Pratsinis, A. Baiker, Oxidative dehydrogenation of ethane with CO_2 over flame-made Ga-loaded TiO_2, ACS Catal. 5 (2015) 690–702, https://doi.org/10.1021/cs500685d.

[28] W. Li, G. Zhang, X. Jiang, Y. Liu, J. Zhu, F. Ding, Z. Liu, X. Guo, C. Song, CO_2 Hydrogenation on unpromoted and M-promoted Co/TiO_2 Catalysts (M = Zr, K, Cs): effects of crystal phase of supports and metal–support interaction on tuning product distribution, ACS Catal. 9 (2019) 2739–2751, https://doi.org/10.1021/acscatal.8b04720.

[29] Q. Li, H. Wang, M. Zhang, G. Li, J. Chen, H. Jia, Suppressive strong metal-support interactions on ruthenium/TiO2 promote light-driven photothermal CO_2 reduction with methane, Angew. Chem. Int. Ed. 62 (2023) e202300129, https://doi.org/10.1002/anie.202300129.

[30] E. Al-Shafei, M. Aljishi, M. Albahar, A. Alahmed, M. Sanhoob, Effect of CO_2/propane ratio and trimetallic oxide catalysts on maximizing dry reforming of propane, Mol. Catal. 537 (2023) 112945, https://doi.org/10.1016/j.mcat.2023.112945.

[31] A. Bermejo-López, B. Pereda-Ayo, J.A. Onrubia-Calvo, J.A. González-Marcos, J. R. González-Velasco, Tuning basicity of dual function materials widens operation temperature window for efficient CO_2 adsorption and hydrogenation to CH_4, J. CO_2 Util. 58 (2022) 101922, https://doi.org/10.1016/j.jcou.2022.101922.

[32] H. Krishna, M.O. Haus, R. Palkovits, Basic silica catalysts for the efficient dehydration of biomass-derived compounds – elucidating structure-activity relationships for Na_2O/SiO_2-type materials, Appl. Catal. B: Environ. 286 (2021) 119933, https://doi.org/10.1016/j.apcatb.2021.119933.

[33] A.L. Petre, A. Auroux, P. Gélin, M. Caldararu, N.I. Ionescu, Acid–base properties of supported gallium oxide catalysts, Thermochim. Acta 379 (2001) 177–185, https://doi.org/10.1016/S0040-6031(01)00615-3.

[34] P. Michorczyk, E. Sikora, J. Ogonowski, Study of the acid-base properties of Ga_2O_3/Al_2O_3 by using test reactions, React. Kinet. Catal. Lett. 94 (2008) 243–252, https://doi.org/10.1007/s11144-008-5296-4.

[35] Y.-x Pan, C.-j Liu, D. Mei, Q. Ge, Effects of hydration and oxygen vacancy on CO_2 adsorption and activation on β-Ga_2O_3(100), Langmuir 26 (2010) 5551–5558, https://doi.org/10.1021/la903836v.

[36] A. Vimont, J.C. Lavalley, A. Sahibed-Dine, C. Otero, Areán, M. Rodríguez Delgado, M. Daturi, Infrared spectroscopic study on the surface properties of γ-gallium oxide as compared to those of γ-alumina, J. Phys. Chem. B 109 (2005) 9656–9664, https://doi.org/10.1021/jp050103+.

[37] S.E. Collins, M.A. Baltanás, A.L. Bonivardi, Infrared spectroscopic study of the carbon dioxide adsorption on the surface of Ga_2O_3 polymorphs, J. Phys. Chem. B 110 (2006) 5498–5507, https://doi.org/10.1021/jp055594c.

[38] A. Boudjemaa, C. Daniel, C. Mirodatos, M. Trari, A. Auroux, R. Bouarab, In situ DRIFTS studies of high-temperature water-gas shift reaction on chromium-free iron oxide catalysts, Comptes Rendus Chim. 14 (2011) 534–538, https://doi.org/10.1016/j.crci.2010.11.007.

[39] A. Erdőhelyi, K. Fodor, G. Suru, Reaction of carbon monoxide with water on supported iridium catalysts, Appl. Catal. A: Gen. 139 (1996) 131–147, https://doi.org/10.1016/0926-860X(95)00316-9.

[40] J. Baltrusaitis, J. Schuttlefield, E. Zeitler, V.H. Grassian, Carbon dioxide adsorption on oxide nanoparticle surfaces, Chem. Eng. J. 170 (2011) 471–481, https://doi.org/10.1016/j.cej.2010.12.041.

[41] C.E. Nanayakkara, W.A. Larish, V.H. Grassian, Titanium dioxide nanoparticle surface reactivity with atmospheric gases, CO_2, SO_2, and NO_2: roles of surface hydroxyl groups and adsorbed water in the formation and stability of adsorbed products, J. Phys. Chem. C. 118 (2014) 23011–23021, https://doi.org/10.1021/jp504402z.

[42] L. Liu, C. Zhao, Y. Li, Spontaneous dissociation of CO_2 to CO on defective surface of Cu(I)/TiO_2–x nanoparticles at room temperature, J. Phys. Chem. C. 116 (2012) 7904–7912, https://doi.org/10.1021/jp300932b.

[43] G. Martra, Lewis acid and base sites at the surface of microcrystalline TiO_2 anatase: relationships between surface morphology and chemical behaviour, Appl. Catal. A: Gen. 200 (2000) 275–285, https://doi.org/10.1016/S0926-860X(00)00641-4.

[44] L. Jin, E. Shaaban, S. Bamonte, D. Cintron, S. Shuster, L. Zhang, G. Li, J. He, Surface basicity of metal@TiO2 to enhance photocatalytic efficiency for CO_2 reduction, ACS Appl. Mater. Interfaces 13 (2021) 38595–38603, https://doi.org/10.1021/acsami.1c09119.

[45] K. Wang, M. Cao, J. Lu, Y. Lu, C.H. Lau, Y. Zheng, X. Fan, Operando DRIFTS-MS investigation on plasmon-thermal coupling mechanism of CO_2 hydrogenation on Au/TiO2: the enhanced generation of oxygen vacancies, Appl. Catal. B: Environ. 296 (2021) 120341, https://doi.org/10.1016/j.apcatb.2021.120341.

[46] J. Szanyi, J.H. Kwak, Dissecting the steps of CO_2 reduction: 1. The interaction of CO and CO_2 with γ-Al2O3: an in situ FTIR study, Phys. Chem. Chem. Phys. 16 (2014) 15117–15125, https://doi.org/10.1039/C4CP00616J.

[47] D. qin, D. Xie, H. Zheng, Z. Li, J. Tang, Z. Wei, In-situ FTIR study of CO_2 adsorption and methanation mechanism over bimetallic catalyst at low temperature, Catal. Lett. 151 (2021) 2894–2905, https://doi.org/10.1007/s10562-021-03539-2.

[48] G. Bampos, T. Ramantani, P. Panagiotopoulou, X.E. Verykios, Effect of support on the reactive adsorption of CO from low CO concentration streams on the surface of Pd based catalysts, Ind. Eng. Chem. Res. 60 (2021) 18722–18738, https://doi.org/10.1021/acs.iecr.1c02710.

[49] C. Weilach, C. Spiel, K. Föttinger, G. Rupprechter, Carbonate formation on Al_2O_3 thin film model catalyst supports, Surf. Sci. 605 (2011) 1503–1509, https://doi.org/10.1016/j.susc.2011.05.025.

[50] W.S. Epling, C.H.F. Peden, J. Szanyi, Carbonate formation and stability on a Pt/BaO/γ-Al_2O3 NO_X storage/reduction catalyst, J. Phys. Chem. C. 112 (2008) 10952–10959, https://doi.org/10.1021/jp712180q.

[51] Z. Wu, A.K.P. Mann, M. Li, S.H. Overbury, Spectroscopic investigation of surface-dependent acid–base property of ceria nanoshapes, J. Phys. Chem. C. 119 (2015) 7340–7350, https://doi.org/10.1021/acs.jpcc.5b00859.

[52] M.A.A. Aziz, A.A. Jalil, S. Wongsakulphasatch, D.-V.N. Vo, Understanding the role of surface basic sites of catalysts in CO_2 activation in dry reforming of methane: a short review, Catal. Sci. Technol. 10 (2020) 35–45, https://doi.org/10.1039/C9CY01519A.

[53] A.A. Davydov, M.L. Shepotko, A.A. Budneva, Basic sites on the oxide surfaces: their effect on the catalytic methane coupling, Catal. Today 24 (1995) 225–230, https://doi.org/10.1016/0920-5861(95)00029-F.

[54] L. Mino, G. Spoto, A.M. Ferrari, CO_2 capture by TiO_2 anatase surfaces: a combined DFT and FTIR study, J. Phys. Chem. C. 118 (2014) 25016–25026, https://doi.org/10.1021/jp507443k.

[55] W. Zhou, Y. Zhang, X. Tao, Y. Zhou, Q. Wei, S. Ding, Effects of gallium addition to mesoporous alumina by impregnation on dibenzothiophene hydrodesulfurization performances of the corresponding NiMo supported catalysts, Fuel 228 (2018) 152–163, https://doi.org/10.1016/j.fuel.2018.04.084.

[56] Z. Shen, J. Liu, H. Xu, Y. Yue, W. Hua, W. Shen, Dehydrogenation of ethane to ethylene over a highly efficient Ga_2O_3/HZSM-5 catalyst in the presence of CO_2, Appl. Catal. A: Gen. 356 (2009) 148–153, https://doi.org/10.1016/j.apcata.2008.12.038.

[57] V. La Parola, L.F. Liotta, G. Pantaleo, M.L. Testa, A.M. Venezia, CO_2 reforming of CH_4 over Ni supported on SiO_2 modified by TiO_2 and ZrO_2: effect of the support synthesis procedure, Appl. Catal. A: Gen. 642 (2022) 118704, https://doi.org/10.1016/j.apcata.2022.118704.

[58] K.N. Papageridis, N.D. Charisiou, S.L. Douvartzides, V. Sebastian, S.J. Hinder, M. A. Baker, S. AlKhoori, K. Polychronopoulou, M.A. Goula, Effect of operating parameters on the selective catalytic deoxygenation of palm oil to produce renewable diesel over Ni supported on Al_2O_3, ZrO_2 and SiO2 catalysts, Fuel Process. Technol. 209 (2020) 106547, https://doi.org/10.1016/j.fuproc.2020.106547.

[59] C.A. Barrales-Cortés, H. Pérez-Pastenes, J.C. Piña-Victoria, T. Viveros-García, Hydrogenation of citral on Pt/SiO_2 catalysts: effect of sn addition and type of solvent, Top. Catal. 63 (2020) 468–480, https://doi.org/10.1007/s11244-020-01312-0.

[60] C.-T. Shao, W.-Z. Lang, X. Yan, Y.-J. Guo, Catalytic performance of gallium oxide based-catalysts for the propane dehydrogenation reaction: effects of support and loading amount, RSC Adv. 7 (2017) 4710–4723, https://doi.org/10.1039/C6RA27204E.

[61] D. Das, H.K. Mishra, K.M. Parida, A.K. Dalai, Preparation, physico-chemical characterization and catalytic activity of sulphated ZrO_2–TiO_2 mixed oxides, J. Mol. Catal. A: Chem. 189 (2002) 271–282, https://doi.org/10.1016/S1381-1169(02)00363-1.

[62] C. Otero Areán, X. Rodrı, M. Guez Delgado, V. Montouillout, J.C. Lavalley, C. Fernandez, J.J. Cuart Pascual, J.B. Parra, NMR and FTIR spectroscopic studies on the acidity of gallia–silica prepared by a sol–gel route, Microporous Mesoporous Mater. 67 (2004) 259–264, https://doi.org/10.1016/j.micromeso.2003.11.009.

[63] A.S. Al-Dughaither, H. de Lasa, HZSM-5 zeolites with different SiO_2/Al_2O_3 ratios. Characterization and NH3 desorption kinetics, Ind. Eng. Chem. Res. 53 (2014) 15303–15316, https://doi.org/10.1021/ie4039532.

[64] P. Castro-Fernández, D. Mance, C. Liu, I.B. Moroz, P.M. Abdala, E.A. Pidko, C. Copéret, A. Fedorov, C.R. Müller, Propane dehydrogenation on Ga2O3-based catalysts: contrasting performance with coordination environment and acidity of surface sites, ACS Catal. 11 (2021) 907–924, https://doi.org/10.1021/acscatal.0c05009.

[65] W. Lueangchaichaweng, N.R. Brooks, S. Fiorilli, E. Gobechiya, K. Lin, L. Li, S. Parres-Esclapez, E. Javon, S. Bals, G. VanTendeloo, J.A. Martens, C.E. A. Kirschhock, P.A. Jacobs, P.P. Pescarmona, Gallium oxide nanorods: novel, template-free synthesis and high catalytic activity in epoxidation reactions, Angew. Chem. Int. Ed. 53 (2014) 1585–1589, https://doi.org/10.1002/anie.201308384.

[66] C. Torres, S. Rostom, H. de Lasa, An eco-friendly fluidizable Fe_xO_y/CaO-γ-Al_2O_3 catalyst for tar cracking during biomass gasification, Catalysts 10 (2020) 806, https://doi.org/10.3390/catal10070806.

[67] J. Mazumder, H. de Lasa, Fluidizable Ni/La_2O_3-γAl_2O_3 catalyst for steam gasification of a cellulosic biomass surrogate, Appl. Catal. B: Environ. 160-161 (2014) 67–79, https://doi.org/10.1016/j.apcatb.2014.04.042.

[68] S.-Z. Zhou, X.-Q. Gao, F. Wu, W.-C. Li, A.-H. Lu, Enriching GaHx species via co-feeding hydrogen to boost efficient propane dehydrogenation over Ga_2O_3/Al_2O_3 catalysts, Appl. Catal. A: Gen. 668 (2023) 119488, https://doi.org/10.1016/j.apcata.2023.119488.

[69] S.A. Al-Ghamdi, H.I. de Lasa, Propylene production via propane oxidative dehydrogenation over VO_x/γ-Al_2O_3 catalyst, Fuel 128 (2014) 120–140, https://doi.org/10.1016/j.fuel.2014.02.033.

[70] X. Wang, J.C. Yu, P. Liu, X. Wang, W. Su, X. Fu, Probing of photocatalytic surface sites on SO_4^{2-}/TiO_2 solid acids by in situ FT-IR spectroscopy and pyridine adsorption, J. Photochem. Photobiol. A: Chem. 179 (2006) 339–347, https://doi.org/10.1016/j.jphotochem.2005.09.007.

[71] F. Lin, Y. Chen, L. Zhang, D. Mei, L. Kovarik, B. Sudduth, H. Wang, F. Gao, Y. Wang, Single-facet dominant anatase TiO_2 (101) and (001) model catalysts to elucidate the active sites for alkanol dehydration, ACS Catal. 10 (2020) 4268–4279, https://doi.org/10.1021/acscatal.9b04654.

[72] S. Songtawee, B. Rungtaweevoranit, C. Klaysom, K. Faungnawakij, Tuning Brønsted and Lewis acidity on phosphated titanium dioxides for efficient conversion of glucose to 5-hydroxymethylfurfural, RSC Adv. 11 (2021) 29196–29206, https://doi.org/10.1039/D1RA06002C.

[73] T.N. Phan, H.-S. Kim, D.-H. Kim, C.H. Ko, Mesoporous titania as a support of gallium-based catalysts for enhanced ethane dehydrogenation performance, Catal. Lett. 151 (2021) 2748–2761, https://doi.org/10.1007/s10562-020-03521-4.

[74] A. Ausavasukhi, T. Sooknoi, D.E. Resasco, Catalytic deoxygenation of benzaldehyde over gallium-modified ZSM-5 zeolite, J. Catal. 268 (2009) 68–78, https://doi.org/10.1016/j.jcat.2009.09.002.

[75] D. Zhao, T. Su, D. Rodríguez-Padrón, H. Lü, C. Len, R. Luque, Z. Yang, Efficient transfer hydrogenation of alkyl levulinates to γ-valerolactone catalyzed by simple Zr–TiO_2 metal oxide systems, Mater. Today Chem. 24 (2022) 100745, https://doi.org/10.1016/j.mtchem.2021.100745.

[76] H. Zhu, Z. Qin, W. Shan, W. Shen, J. Wang, Pd/CeO_2–TiO_2 catalyst for CO oxidation at low temperature: a TPR study with H_2 and CO as reducing agents, J. Catal. 225 (2004) 267–277, https://doi.org/10.1016/j.jcat.2004.04.006.

[77] J. Liu, J. Yue, M. Lv, F. Wang, Y. Cui, Z. Zhang, G. Xu, From fundamentals to chemical engineering on oxidative coupling of methane for ethylene production: a review, Carbon Resour. Convers. 5 (2022) 1–14, https://doi.org/10.1016/j.crcon.2021.11.001.

[78] K. Ishimaru, T. Hata, P. Bronsveld, T. Nishizawa, Y. Imamura, Characterization of sp2- and sp3-bonded carbon in wood charcoal, J. Wood Sci. 53 (2007) 442–448, https://doi.org/10.1007/s10086-007-0879-7.

[79] J. Jana, T. Van Phuc, J.S. Chung, W.M. Choi, S.H. Hur, Nano-dimensional carbon nanosphere supported non-precious metal oxide composite: a cathode material for sea water reduction, Nanomaterials 12 (2022) 4348, https://doi.org/10.3390/nano12234348.

[80] I.V. Yentekakis, G. Goula, M. Hatzisymeon, I. Betsi-Argyropoulou, G. Botzolaki, K. Kousi, D.I. Kondarides, M.J. Taylor, C.M.A. Parlett, A. Osatiashtiani, G. Kyriakou, J.P. Holgado, R.M. Lambert, Effect of support oxygen storage capacity on the catalytic performance of Rh nanoparticles for CO_2 reforming of methane, Appl. Catal. B: Environ. 243 (2019) 490–501, https://doi.org/10.1016/j.apcatb.2018.10.048.

[81] M. Rezaei, S.M. Alavi, S. Sahebdelfar, Z.-F. Yan, Syngas production by methane reforming with carbon dioxide on noble metal catalysts, J. Nat. Gas. Chem. 15 (2006) 327–334, https://doi.org/10.1016/S1003-9953(07)60014-0.

[82] C.H. Bartholomew, Mechanisms of catalyst deactivation, Appl. Catal. A: Gen. 212 (2001) 17–60, https://doi.org/10.1016/S0926-860X(00)00843-7.

[83] B. Xu, T. Li, B. Zheng, W. Hua, Y. Yue, Z. Gao, Enhanced stability of HZSM-5 supported Ga_2O_3 catalyst in propane dehydrogenation by dealumination, Catal. Lett. 119 (2007) 283–288, https://doi.org/10.1007/s10562-007-9232-4.